Consequences of excessive glucosylsphingosine in glucocerebrosidase-deficient zebrafish.

Lindsey T. Lelieveld[1], Sophie Gerhardt[2], Saskia Maas[2], Kimberley C. Zwiers[1], Claire de Wit[1], Ernst H. Beijk[3], Maria J. Ferraz[1], Marta Artola[1], Annemarie H. Meijer[3], Christian Tudorache[3], Daniela Salvatori[2,4], Rolf G. Boot[1], and Johannes M. F. G. Aerts[1]*

[1]Medical Biochemistry, Leiden Institute of Chemistry, Leiden University, Leiden, The Netherlands; [2]Pathology Unit, Central Laboratory Animal Facility, Leiden University Medical Center, Leiden, The Netherlands; [3]Institute of Biology, Leiden University, Leiden, The Netherlands; [4]Anatomy and Physiology, Clinical Sciences, Faculty of Veterinary Medicine, Utrecht University, Utrecht, The Netherlands

Abstract In Gaucher disease (GD), the deficiency of glucocerebrosidase causes lysosomal accumulation of glucosylceramide (GlcCer), which is partly converted by acid ceramidase to glucosylsphingosine (GlcSph) in the lysosome. Chronically elevated blood and tissue GlcSph is thought to contribute to symptoms in GD patients as well as to increased risk for Parkinson's disease. On the other hand, formation of GlcSph may be beneficial since the water soluble sphingoid base is excreted via urine and bile. To study the role of excessive GlcSph formation during glucocerebrosidase deficiency, we studied zebrafish that have two orthologs of acid ceramidase, Asah1a and Asah1b. Only the latter is involved in the formation of GlcSph in glucocerebrosidase-deficient zebrafish as revealed by knockouts of Asah1a or Asah1b with glucocerebrosidase deficiency (either pharmacologically induced or genetic). Comparison of zebrafish with excessive GlcSph ($gba1^{-/-}$ fish) and without GlcSph ($gba1^{-/-}$:$asah1b^{-/-}$ fish) allowed us to study the consequences of chronic high levels of GlcSph. Prevention of excessive GlcSph in $gba1^{-/-}$:$asah1b^{-/-}$ fish did not restrict storage cells, GlcCer accumulation, or neuroinflammation. However, GD fish lacking excessive GlcSph show an ameliorated course of disease reflected by significantly increased lifespan, delayed locomotor abnormality, and delayed development of an abnormal curved back posture. The loss of tyrosine hydroxylase 1 (*th1*) mRNA, a marker of dopaminergic neurons, is slowed down in brain of GD fish lacking excessive GlcSph. In conclusion, in the zebrafish GD model, excess GlcSph has little impact on (neuro)inflammation or the presence of GlcCer-laden macrophages but rather seems harmful to *th1*-positive dopaminergic neurons.

Supplementary key words Gaucher disease • acid ceramidase • lipid metabolism • zebrafish • glucosylceramide • sphingolipids • lysosphingolipids • dopaminergic neurons

*For correspondence: Johannes M. F. G. Aerts, j.m.f.g.aerts@LIC. leidenuniv.nl.

Gaucher disease (GD), one of the most common inherited lysosomal storage disorders, is caused by deficient activity of lysosomal glucocerebrosidase (GCase), encoded by the *GBA1* gene (1). The nature and severity of clinical manifestations is remarkably diverse among GD patients, ranging from perinatal to adult phenotypes (1). Numerous mutations in *GBA1* have been identified and carrier frequencies as high as 1 in 50 individuals have been observed (2–4). GD is particularly prevalent among Ashkenazi populations with a reported incidence of 1 in about 1,000 live births (5). The association between mutations in *GBA1* and the development of parkinsonism was first noted in the 1990's, and it became clear that Parkinson disease was more common in heterozygote family members of patients with GD (6, 7). The various pathophysiological mechanisms involved in manifestation of GD symptoms and risk for PD are not well understood. The physiological substrate of GCase is the ubiquitous glycosphingolipid (GSL) glucosylceramide (GlcCer) that is cleaved by the enzyme into ceramide (Cer) and glucose in the lysosome (1). Macrophages in spleen, liver, and bone marrow of GD patients prominently store GlcCer in their lysosomes thus transforming into characteristic Gaucher cells (8). These storage macrophages are viable and secrete specific proteins into the circulation such as the enzyme chitotriosidase, the chemokine CCL18, and a soluble fragment of the transmembrane glycoprotein gpNMB (9–11) and their plasma levels reflect the body burden of lipid-laden macrophages in GD patients (12–14). Gaucher cells are also the main source of more than hundred-fold elevated glucosylsphingosine (GlcSph) in plasma of GD patients (15). It has been speculated that excessive GlcSph contributes to signs and symptoms of Gaucher disease, including chronic B cell activation and proliferation, aggregation of α-synuclein in PD, impairment of osteoblasts, and disturbance of cerebral microvasculature (16–20). Consistently, repeated intravenous administration of a

relative high dose of GlcSph to mice was found to induce formation of lipid-laden storage cells as well as hepatosplenomegaly and hematological symptoms seen in GD patients, although in more modest manner than in mice with an inducible GCase deficiency in the white blood cell lineage (21, 22). Although these findings suggest direct and concentration-dependent toxicity of GlcSph, interpretation of the observations is complicated by the fact that high concentrations of GlcSph as such inhibit GCase (23). Many studies examining the toxicity of GlcSph have been performed using exogenously added GlcSph. It is unclear whether similar GlcSph levels are reached in this manner as the endogenous ones in the cells of GD patients.

We earlier provided genetic and pharmacological evidence for the key role of acid ceramidase (ACase; N-acylsphingosine deacylase; E.C. 3.5.1.23) in the excessive formation of GlcSph during GCase deficiency (24). It was shown that fibroblasts from Farber patients, with inherited deficiency of ACase, do not form GlcSph upon inactivation of GCase as WT cells do, confirming an earlier observation by Kobayahsi et al (25). ACase is encoded by the *ASAH1* gene located on chromosome 8. ACase deficiency can lead to the severe lysosomal storage disorder Farber disease (FD) characterized by deformed joints, subcutaneous nodules, progressive hoarseness, and progressive neurological symptoms. In classic FD patients, cells show less than 10% residual ACase activity. In spinal muscular atrophy with progressive myoclonic epilepsy, ACase activity is also reduced, but the residual activity is higher, as much as 32% of normal activity (26, 27). ACase normally hydrolyzes Cer with a pH optimum of 4.5–5, rendering sphingosine and a free fatty acid as products (28). ACase is a heterodimer consisting of an α-subunit (13 kDa) and a β-subunit (40 kDa) linked via a disulfide bridge (29). The enzyme is initially synthesized as N-glycated precursor and transported to lysosomes via mannose-6-phosphate–mediated sorting. Inside the lysosome, ACase is processed by autocleavage into the α and β subunits, thereby freeing the catalytic cysteine residue at the novel N-terminus of the β-subunit and triggering a conformational change that opens up the active site for substrate entry (30–32).

Zebrafish offer an attractive model to study GlcCer metabolism since the key enzymes in synthesis and degradation are similar to those in humans. We recently successfully generated CRIPSR/Cas9 zebrafish lacking lysosomal GCase (33). In contrast to mammalian species, the complete GCase-deficient fish are viable. Like GD disease patients, these fish rapidly develop increased levels of GlcSph (15). In addition, we developed small compounds that allow rapid, on-demand inactivation of GCase in different species including zebrafish (34). Based on sequence homology, there are two zebrafish homologs of human lysosomal ACase: Asah1a and Asa1b (35–37); one homolog of ASAH2, neutral ceramidase: Asah2; and, three alkaline ceramidases as in the ones man (ACER1-3): Acer1-3. *Danio* therefore seems to contain six ceramidases, of which only the Asah1a and Asha1b contain a classical signal peptide, all the others lack this. Morpholino knockdown of *asah1b* in zebrafish led to loss of motor neuron axonal branching and spinal cord degeneration (36). The morphants showed considerable residual ACase activity but no Cer accumulation (36). Recently, double *asah1a:asah1b* KO zebrafish were generated using CRISPR/Cas9 technology: these mutant fish were significantly smaller than WT, had a shorter life-span, and showed accumulation of Cer (37).

The aim of our present investigation with zebrafish was to further elucidate the detrimental role of excessive GlcSph formed during GCase deficiency at organismal level. For this purpose, we first generated gene knockouts of *asah1a* and/or *asah1b* to establish which enzyme is responsible for the formation of GlcSph in GCase-deficient zebrafish. Fortuitously, only Asah1b was found to be involved in GlcSph formation during GCase deficiency. This allowed us to generate GCase-deficient fish ($gba1^{-/-}:asah1b^{-/-}$) that do not produce excessive GlcSph and at the same time show no major abnormality in Cer levels. We next compared GCase-deficient fish with or without GlcSph ($gba1^{-/-}:asah1b^{+/+}$ and $gba1^{-/-}:asah1b^{-/-}$ fish). Our investigation revealed phenotypic improvements in GD fish lacking endogenous GlcSph without a significant change in lipid-laden macrophages and GlcCer accumulation, inflammation, and complement cascade activation.

MATERIALS AND METHODS

Chemicals and reagents

GCase specific inhibitor (ME656) (34), $^{13}C_5$-sphinganine, $^{13}C_5$-sphingosine, $^{13}C_5$-GlcSph, $^{13}C_5$-lyso-globotriaosylceramide (LysoGb3), Cl7-lysosphingomyelin (LysoSM), $^{13}C_6$-GlcChol, and Cl7-dihydroceramide (38, 39) were synthesized as reported. All chemicals and reagents were obtained from Sigma-Aldrich (St Louis, USA) unless mentioned otherwise. The standards Cer (d18:1/16:0), dhCer (d18:0/16:0), GlcCer (d18:1/16:0), galactosylceramide (GalCer) (d18:1/16:0), and LacCer (d18:1/16:0) were obtained from Avanti Polar lipids (Alabaster, USA) and glucosylated cholesterol (GlcChol) from Sigma-Aldrich. LC-MS grade methanol, 2-propanol, water, formic acid, acetonitrile, and HPLC grade chloroform were purchased from Biosolve (Valkenswaard, the Netherlands). LC-MS grade ammonium formate, ammonium acetate, and sodium hydroxide from Sigma-Aldrich, and butanol and hydrochloric acid from Merck Millipore (Billerica, USA).

Cloning and cell culture

Gateway Technology (Thermo Fisher) was used according to the manufacturer's instructions to create constructs. Generation of the pLenti6.3/V5 destination with the human *ASAH1* coding sequence was described before (24). Coding sequences of *asah1a* and *asah1b* were amplified by PCR using primers flanked with attB sites (supplemental Table S1). The attB PCR product was shuttled into a pDONR™221 vector using the BP recombination reaction and subcloned into the

pLenti6.3/V5-DEST destination gateway vector. All constructs were validated using Sanger sequencing.

Cell culture, transfection of human embryonic kidney 293T (HEK293T) cells, infection of Farber fibroblasts, and selection of fibroblasts stably overexpressing ACase was performed according to the protocol described before (24). Briefly, HEK293T cells were grown in Dulbecco's Modified Eagle's Medium (DMEM) supplemented with 10% (v/v) Fetal Calf Serum, 0.1% (w/v) penicillin/streptomycin, and 1% (v/v) Glutamax in a 5% CO_2 humidified incubator at 37°C. Fibroblasts obtained from FD patients were grown in DMEM/Nutrient mixture F-12 (DMEM/F12) supplemented with 10% (v/v) Fetal Calf Serum, 0.1% (w/v), penicillin/streptomycin, and 1% (v/v) Glutamax in a 5% CO_2 humidified incubator at 37°C. HEK293T cells were transfected with a control pLenti6.3 construct (expressing GFP) or the different pLenti6.3-ASAH1 constructs in combination with viral packaging vectors (pMD2.G, pMDLg/pRRe and pRSV-Rev) and poly-ethyleneimine (PEI) to produce lentiviral particles that were subsequently collected and used for infection of the Farber fibroblast cell line. Fibroblasts were incubated with the lentiviral particles for 48 h. Farber Fibroblast cells stably expressing the human ACase, Asah1a, or Asah1b were selected by incubation medium supplemented with blasticidin for several passages.

Farber fibroblasts inhibitor incubation

Fibroblasts were seeded in a 12-well plate at a ratio of 0.5 × 10^6 cells/well one day prior to incubation.Control Farber fibroblasts (overexpressing GFP) or Farber fibroblasts stably overexpressing human ACase, Asah1a, or Asah1b were incubated with either vehicle (1% (v/v) DMSO) or the GCase specific inhibitor (9.6 nM ME656, 1% (v/v) DMSO). After 24 h, the cells were washed three times with ice cold PBS and harvested in 120 µl of ice-cold water. Homogenate preparation, determination of the protein concentration, and lipid extraction was performed as described below.

Zebrafish

All zebrafish were housed and maintained at the University of Leiden, the Netherlands, according to standard protocols (zfin.org) and following the guidelines of the Animal Welfare Body. WT zebrafish (ABTL) were a mixed lineage of WT AB and WT Tüpfel Long Fin genetic backgrounds. CRISPR/Cas9-mediated mutant zebrafish were crossed at least 2 times with WT fish before generating the double heterozygous line. These crossings were performed to obtain a diverse genetic background as observed in WT zebrafish (40). Zebrafish were kept at a constant temperature of 28.5°C and on a cycle of 14 h light and 10 h dark. Experiments with larvae, juvenile, and adult zebrafish after the free-feeding stage were in line with the European Directive 201/63/EU and approved by the Dutch Central Commission for Animal experimentation (Centrale Commissie voor Dierproeven, project license AVD1060020184725). Zebrafish from the age of 5 days postfertilization (dpf) to 2 weeks postfertilization (wpf) were fed with both dry food (2× daily; Skretting Gemma micro 75, Zebcare, Nederweert, the Netherlands) and Rotifers (1× daily) and fed with both dry food (2× daily; Skretting Gemma micro 150 until 30 dpf or Gemma Micro 300 mixed with Gemma Diamond for fish from 30 dpf) and hatched Artemia (1× daily) from 3 wpf to the end of the experiment.

CRISPR/Cas9-mediated KO of *asah1a* and *asah1b*

CRISPR/Cas9-mediated *gba1* KO zebrafish were generated and maintained as previously described (33). CRISPR/Cas9-mediated zebrafish gene KOs of *asah1a* and *asah1b* were generated using the protocol previously described (33) with sgRNA1 5′-gGTGTCCATCTCTCACTAGG and sgRNA2 5′-GgGCTTCCCGCTGGGAACAA for *asah1a* and *asah1b*, respectively. Of note, the first or second nucleotide of the sgRNA found by the CHOPCHOP webtool is replaced by a 'g' to improve T7 RNA synthesis. Injected founders were crossed to WT and their off-spring screened using an high resolution melt assay with primers described in supplemental Table S1, and fragments for Sanger sequencing were obtained using primers also described in supplemental Table S1. Heterozygous adult zebrafish (F2 generation) of both genotypes were crossed to obtain double heterozygous zebrafish ($asah1a^{+/-}:asah1b^{+/-}$). Adult fish were crossed with each other, and off-spring was used for incubations with vehicle (0.1% DMSO) or GCase specific inhibitor (10 µM ME656, 0.1% DMSO) for 5 days, followed by (glyco)sphingolipid analysis. The $gba1^{-/-}$, $gba1^{+/+}:asah1b^{-/-}$,and $gba1^{-/-}:asah1b^{-/-}$ zebrafish were generated by appropriate crossings. The status of *gba1* and *asah1b* was determined by fin clipping of 4–5 dpf larvae and subsequent high resolution melt assays.

Fish lacking only one of the ACase enzymes was maintained for crossings and lived as long as WT fish, with no clear changes in swimming behavior, feeding behavior, and morphology such as size, weight, curvature, and general appearance.

Zebrafish sampling

Zebrafish were sacrificed at 12 wpf or earlier when zebrafish showed symptoms noted as human endpoints. From 8 wpf, zebrafish were monitored extensively for phenotypic and morphological symptoms such as curvature of the back and abnormal swimming behavior. Humane endpoints were defined as follows: 1) fish having a moderate to extreme curvature of the spine independent of the feeding consumption, 2) fish with a slight curvature but clear abnormal swimming behavior, or 3) fish with a slight curvature which are unable to reach and consume the provided food. $Gba1^{-/-}$ zebrafish were sacrificed between 10 and 12 wpf, while no symptoms were observed for WT, $asah1b^{-/-}$, and $gba1^{-/-}:asah1b^{-/-}$. The same humane endpoints were used for the longevity study of the $gba1^{-/-}:asah1b^{-/-}$. Individual zebrafish were transferred to single tanks (1 1 external breeding tank with lid, Techniplast, West Chester, USA) acclimatized for 10 min and recorded from the side for 20 min. Fish were sacrificed using an overdose of tricaine methane sulfonate (MS222, 200 mg/L) and photographed using a Leica M165C microscope (Wetzlar, Germany). Whole zebrafish were fixed for histopathology as described below, or organs were dissected. Dissected organs were either snap frozen in liquid nitrogen for protein and (glyco)sphingolipid analysis or submerged in RNAlater™ (Invitrogen, Thermo Fisher Scientific, Waltham USA) for RT-PCR analysis (brain or liver) and stored at −80°C.

Movement analysis

The individual tanks were randomly placed in a 3 × 4 or 4 × 4 setup, and the camera was placed at a distance dependent on the setup to include all tanks. Zebrafish were left for at least 10 min to acclimatize and recorded for 20 min using a Sony A6000 camera (Tokyo, Japan) with a 30 mm objective.

Movements of the fish in the individual tank were tracked using Ethiovision software 10.1 (Noldus, Wageningen, the Netherlands). Arenas were setup for each individual tank by drawing a rectangular shape in the tank, thereby not including any reflections at the top, bottom, and sides. The arenas without reflection accompanied approximately 46 ± 5% of the total area of the individual tank (± 17 cm length × 8 cm weight). A horizontal and vertical line were used to calibrate the area to the measurements of the tank, and each arena was divided in two equal zones: a top and bottom zone. The detection settings were set as follows: model-based and differencing settings for Nose-tail detection; the subject color was brighter than background, sensitivity of 45; subject size with a minimum of 80 and maximum of 2042 pixels and video sample rate of 6.25 per sec. Data was acquired every 0.16 s for a total of 10 min after a 5 min delay. The data was exported, and the velocity was calculated by averaging the velocity of all datapoints, while the time spend in the bottom zone was obtained by dividing the amount time spend in the bottom zone by the total time.

Zebrafish morphology

The three or four images of one fish, obtained with the Leica microscope, were stitched to obtain one image using Photoshop CC2018 (Adobe, San Jose, USA). The length of the fish from head to tail base (body length) was determined as well as the length of the back from head to tail base (long length) using ImageJ software (41). The tortuosity was calculated by dividing the long length by the body length.

Homogenate preparation

Homogenates of brain and liver samples were prepared in potassium phosphate lysis buffer (25 mM K_2HPO_4-KH_2PO_4 pH 6.5, 0.1% (v/v) Triton-X100 and EDTA-free protease inhibitor (cOmplete™, EDTA-free Protease Inhibitor Cocktail, Roche, Sigma-Aldrich)). Organs were first homogenized using a Dounce homogenizer (10 strokes) followed by sonication (20% amplitude, for 4 cycles of 3 s on and 3 s off) using a Vibra-Cell™ VCX 130 (Sonics, Newtown, USA) while placing the samples on ice. Total protein concentration of homogenates was determined using Pierce™ BCA protein assay kit (Thermo Fisher Scientific, Waltham, USA) and measured using an EMax® plus microplate reader (Molecular Devices, Sunnyvale, USA).

Western blot

Proteins of brain homogenates (20 μg protein) were denatured using 5x Laemmli sample buffer (25% (v/v) 1.25 M Tris-HCL pH 6.8, 50% (v/v) 100% glycerol, 10% (w/v) sodium dodecyl sulfate, 8% (w/v) DTT, and 0.1% (w/v) bromophenol blue), samples were boiled for 5 min at 98°C, and proteins were separated by electrophoresis on a 12% (w/v) SDS-PAGE gel. Proteins were transferred to nitrocellulose membranes (0.2 μM, Bio-Rad laboratories Inc., Hercules, USA) using the Trans-Blot® Turbo™ Transfer system (Bio-Rad). Membranes were blocked with 5% (w/v) BSA and incubated overnight at 4°C with primary antibodies: rabbit anti-LC3 (1:1000, NB100-2220; Novus Biologicals, Centennial, USA), rabbit anti-p62/SQSTM1 (1:1000, P0067; Sigma-Aldrich), or rabbit anti-actin (1:1000, ab209857; Abcam, Cambridge, UK). Membranes were washed 3 times with TBST and incubated for 1 h at RT with secondary antibody: GARPO goat anti rabbit IgG (H+L) peroxidase (1:5000, Bio-Rad). Chemiluminescence signal was developed using the Clarity Max Western ECL substrate (Bio-Rad), detected using a ChemiDocMP imager (Bio-Rad) and the signal quantified by ImageJ software.

Gene expression analysis

RNAlater™ was removed from stored brain and liver samples, and RNA was extracted using a Nucleospin RNA XS column (Machinery-Nagel, Düren, Germany) procedure according to supplier's protocol, without the addition of carrier RNA. Contaminating DNA was degraded on column by a DNase I treatment (supplied in the kit). cDNA was synthesized using SuperScript™ II reverse transcriptase (Invitrogen, Thermo Fisher Scientific, Waltham, USA) using oligo(dT) and an input of approximately 200–500 ng total RNA according to the manufacturer's instruction. Generated cDNA was diluted to an approximate concentration of 0.5 ng total RNA input/μl with Milli-Q water. RT-PCR reactions were performed with the IQ SYBR green mastermix (Bio-Rad laboratories Inc., Hercules, USA) in a total volume of 15 μl (1x SYBR green, 333 μM of forward and reverse primer as given in supplemental Tables S1 and 5 μl of the diluted cDNA input) and carried out using a CFX96™ Real-Time PCR Detection system (Bio-Rad laboratories Inc., Hercules, USA) with the following conditions: denaturation at 95°C for 3 min, followed by 40 cycles of amplification (95°C for 30 s and 61°C for 30 s), imaging the plate after every extension at 61°C, followed by a melt program from 55–95°C with 0.5°C per step with imaging the plate every step. Differential gene expression of each biological sample was calculated using the ΔΔCτ method normalized to two house-keeping genes *ef1a* and *rpl13* and depicted as fold change compared to WT.

(Glyco)sphingolipid analysis

Neutral (glyco)lipids, (glyco)sphingoid bases, and glycosylated cholesterol were extracted from zebrafish larvae, cell- or tissue-homogenates using an acidic Bligh and Dyer procedure (1/1/0.9 chloroform/ methanol/ 100 mM formate buffer pH 3.1) as described before (33, 39). Lipids were resuspended in methanol, when using a C18 column, or acetonitrile/methanol (9/1, v/v) when using a HILIC column, and transferred to a vial for LC-MS/MS analysis. LC-MS/MS measurements were performed using a Waters UPLC-Xevo-TQS micro instrument (Waters, Corporation, Milford, USA) in positive mode using an electrospray ionization source as described before for separating GlcChol and (glyco)sphingolipids using the C18 column (26, 42, 43). To separate glucolipids and galactolipids by HILIC chromatography, a BEH HILIC column (2.1 × 100 mm with 1.7 μm particle size, Waters) was used at 30°C as described before (26) with minor modifications in the eluent program allowing a faster run while preserving the separation of Glc- and Gal-containing lipids. Eluent A contained 10 mM ammonium formate in acetonitrile/water (97:3, v/v) with 0.01% (v/v) formic acid, and eluent B consisted of 10 mM ammonium formate in acetonitrile/water (75:25, v/v) with 0.01% (v/v) formic acid. Lyso- and deacylated-glycosphingolipids were eluted in 10 min with a flow of 0.6 ml/min using the following program: 85% A from 0–1 min, 85%–65% A from 1-2.5 min, 60%–0% A from 2.5–4 min, 0% A from 4–4.5 min, 0%–85% A from 4.5–4.6 min, and re-equilibration with 85% A from 4.6–10 min. GlcChol was eluted in 18 min with a flow of 0.25 ml/min using the following program: 100% A from 0–3 min, 100%–0 % A from 3–3.5 min, 0% A from 3.5–4.5 min, 0%–100% A from 4.5–5 min, and re-equilibration with 100% A from 5–18 min. Lipid levels

were calculated in pmol/mg total protein, sphingoid bases and GlcChol were calculated based on the respective isotopic ^{13}C internal standard, while deacylated neutral (glyco)sphingolipids were calculated using C17-dhCer as internal standard and normalized using the respective standard.

Histology

For histopathology, sacrificed zebrafish were opened along the ventral line and subsequently fixed in paraformaldehyde (4% PFA (w/v), Alfa Aesar, Haverhill, USA) overnight or Bouin's solution (5% acetic acid, 9% formaldehyde, 0.9% picric acid, Sigma-Aldrich) for 4 days, decalcified for 4 days using formic acid (20% (v/v)), and embedded in paraffin. Subsequently, serial sections of 5 μM thickness were made using a Leica RM2055 microtome. For H&E staining, the sections were stained with hematoxylin and eosin. For immunostaining, brain sections were rehydrated and treated with citric buffer (10 mM citric acid buffer, pH 6.) at 98°C. Endogenous peroxidases were inhibited by treatment with 0.3% H_2O_2 in PBS. Next, the sections were incubated with L-plastin primary antibody, to visualize immune cells, in PBST/1% BSA (1:500, GTX124420; Genetex Inc., Irvine, USA), subsequently incubated with the secondary antibody (1:200, goat anti-Rabbit-biotin, BA-1000; Vector laboratories, Burlingame, USA) and finally incubated with ABC reagent. Sections were developed using DAB solution, counterstained with hematoxylin, dehydrated and mounted using Entellan®. The slides were examined using light microscopy.

Sequence alignment and modeling

Signal peptides were predicted using the SignalP-5.0 server (44) and sequences aligned with Clustal Omega (45). Signal peptides were excluded and Asah1a or Asah1b structures were modeled with Swiss-Model (46) using human ACase, PDB 6MHM (32), as search model. The structures were superimposed and visualized with CCP4MG (47).

Statistical analyses

Statistical analyses were performed using GraphPad Prism (v8.1.1, GraphPad software, CA, USA) and data depicted as described in the result section. The data of lipid, protein, and mRNA levels was analyzed by One-Way Anova using Dunnett's test, with WT as control group, or Tukey's multiple comparison test as described in the result section. The data of length and tortuosity were analyzed using a nonparametric Kruskal–Wallis test with Dunn's multiple comparison. In general, statistical comparisons are performed on WT versus $gba1^{-/-}$, WT versus $gba1^{-/-}:asah1b^{-/-}$, and $gba1^{-/-}$ versus $gba1^{-/-}:asah1b^{-/-}$, and depicted only when a significant difference is apparent and relevant. Ns = not significant, $*p < 0.05$, $**p < 0.01$, $***p < 0.001$, and $****p < 0.0001$.

RESULTS

Two Acase orthologs in zebrafish: asah1a and asah1b

Danio rerio has two homologous *asah1* genes encoding ACase enzymes: Asah1a (UniProt accession Q5XJR7) and Asah1b (UniProt accession Q6PH71). The aligned protein sequences of human ACase (UniProt accession Q13510), Asah1a, and Asah1b reveal similarities and differences between the enzymes (**Fig. 1**). The predicted Asah1a protein has 59% identity to the human protein, the Asah1b has 60% identity, and the zebrafish ACase proteins have 70% identity to each other. The predicted signal peptide showed the most variation (depicted in blue) (44). Four potential N-glycosylation sites are present in both zebrafish Asah1 proteins (Asn173, Asn259, Asn286, and Asn342 of human ACase, depicted in yellow) (31). The catalytic cysteine (Cys143) in human ACase, at the free N-terminus of the β-subunit after autocleavage, is present in a highly conserved region of both zebrafish Asah1 proteins (Fig. 1). The α- and β-subunit of the mature heterodimeric human ACase protein are linked by a disulfide bond of Cys31 and Cys340, both being conserved in the zebrafish Asah1a and Asah1b proteins. Important residues in the β-subunit of human ACase, such as Arg159, Asp162, Glu225, and Asn320, are conserved in both zebrafish proteins (green and orange for Arg/Asp and Glu/Asn, respectively). These amino acids are thought to play roles in stabilizing the catalytic N-terminus and/or positioning the Cer substrate during hydrolysis (31). *In silico* modeling of human and zebrafish enzymes reveals that Asah1a contains more aromatic residues lining the entrance of the pocket (supplemental Figs. S1 and S2). However, none of these residues seem to be in close proximity to the catalytic site.

Only double *asah1a:asah1b* larvae accumulate the primary substrate Cer

Next, CRISPR/Cas9-mediated KOs of Asah1a and Asah1b were generated to study the role of both zebrafish ACases in vivo. SgRNA sequences were selected in the third exon of *asah1a*, located on chromosome 14, and the fourth exon of *asah1b* located on chromosome 1 (**Fig. 2**A, B, top and middle panels). Injection of Cas9 mRNA and the appropriate sgRNA in the single-cell stage of WT embryos resulted in founder fish with a germline transmitted deletion of 8 bp for *asah1a* and an insertion of 11 bp for *asah1b* (Fig. 2A, B, lower panels). The predicted stop-codons of these mutations are located in exon 3 and exon 4 for *asah1a* and *asah1b*, respectively, both in the translated α-subunit (mutation marked in Fig. 1 with an arrow).

Double heterozygous $asah1a^{+/-}:asah1b^{+/-}$ zebrafish were crossed, and lipid analysis of WT, $asah1a^{-/-}$, $asah1b^{-/-}$, and $asah1a^{-/-}:asah1b^{-/-}$ larvae (5 dpf) showed that Cer was only significantly increased in double mutant $asah1a^{-/-}:asah1b^{-/-}$ fish (**Fig. 3**A). This finding indicates that Asah1a and Asah1b enzymes are both able to hydrolyze Cer and that the presence of either Asah1a or Asah1b sufficiently degrades Cer and prevents its accumulation. Parallel to our study, Zhang et al. (37) reported the generation of Farber fish by combined CRISPR/Cas9-mediated knockouts of Asha1a and Asah1b. They meticulously analyzed the accumulating Cer species by parallel reaction monitoring LC-MS/MS. The authors noted that Asah1b KO fish have no prominent Cer accumulation (37).
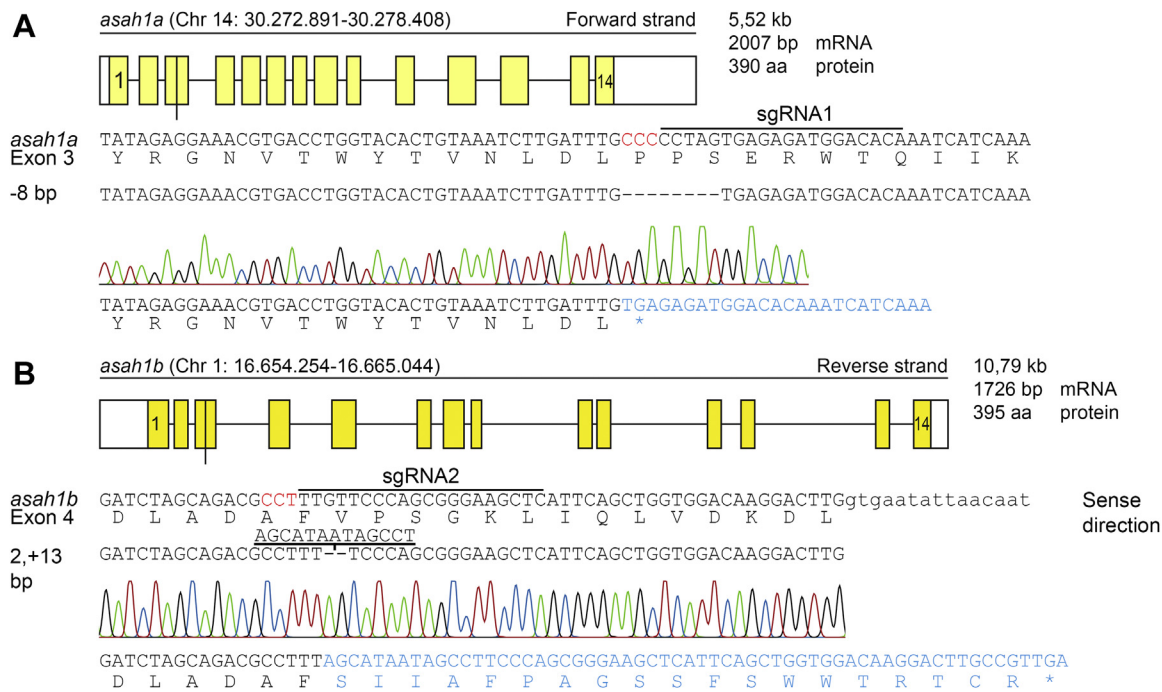
```
                                                        |30                        ↓1a⁻⁸
hACase   MPGRSCVALV-LLAAAVSCAVAQHAPPWTEDCRKSTYPPSGPTYRGAVPWYTINLDLPPY   59
Asah1a   ----MKLVFRYNALFISIFIHALYV-QGLEDCRSGMYPPKGPTYRGNVTWYTVNLDLPPS   55
Asah1b   MNNRLNLCFFI-LSYMCMCLSAQYVPPFTEDCRSGMYPPNGPTFKGDVSWYTVDLDLPAS   59
         : :       :.        * :.    ****.. ***.***::* * ***::****

                         ↓1b⁺¹¹
hACase   KRWHELMLDKAPVLKVIVNSLKNMINTFVPSGKIMQVVDEKLPGLLGNFPGPFEEEMKGI   119
Asah1a   ERWTQIIKDKNTELIEMVQTIKDMAKGFF-HGKLVNFVDKELPFIVDTLPNPFNEEIKGI   114
Asah1b   KRWTDVISDKKTEMASMIQAIRDLADAFVPSGKLIQLVDKDLPLMVDTLPYPFNEEIRGI   119
         :** ::: **    :   :::::::: . *.   **::.**:.** ::..:* **:**::**

                              ▽
hACase   AAVTDIPLGEIISFNIFYELFTICTSIVAEDKKGHLIHGRNMDFGVFLGWNINNDTWVIT   179
Asah1a   AAVSGIPLGEIALFNIFYEVFTVCTSLVAEDNNGNIYHGRNLDFGLFMGWDRQNKTWTLT   175
Asah1b   ASVSGVPLGEVVLFNIFYEVFTVCTSLVAEDVNGNLIHARNLDFGLFMGWDLKNRSWVIT   179
         *:*:.:****:  *******:**:***:**** :*:: *.**:***:*:**: :* :*..:*

                              |200                 |220
hACase   EQLKPLTVNLDFQRNNKTVFKASSFAGYVGMLTGFKPGLFSLTLNERFSINGGYLGILEW   239
Asah1a   EKLKPLVVNINFERKNQTVFKSTSFAGYVGMLTGIRPGELTLTMNERFDFDGGYIGILDW   235
Asah1b   EKLKPLVVNIDFTRNGQTVFKSTNFAGYVGMLTGIHQNSFTLTMNERFSLDGGYIGILEW   239
         *:****.**::* *:..:***::.***********:: . ::**:****.::***:***:*

                              |260           |280
hACase   ILGKKDVMWIGFLTRTVLENSTSYEEAKNLLTKTKILAPAYFILGGNQSGEGCVITRDRK   299
Asah1a   IFGNRDGMWTGFLTRRVLENSTSYEDAKDQLSQTKLLAPVYFILGGNRTGQGCVITRTRI   294
Asha1b   ILGKRDGMWMSFLTRSVLENATSYESAKALLSDTKLLAPAYFILGGNQSGEACIITRSRT   299
         *:*::* ** .**** ****:****.**  *:.**:***.*******::*:.*:*** *

                              |320           |340
hACase   ESLDVYELDAKQGRWYVVQTNYDRWKHPFFLDDRRTPAKMCLNRTSQENISFETMYDVLS   359
Asah1a   NTLDIWELELMLGRWYVLETNYDHWDKPMFLDDRRTPAMKCMNQTTQANISLASIYNVLS   355
Asah1b   QNISPLELNVKNGRWYVLETNYDHWKEPLFLDDRRTPAMKCMNQTTQTNISVKTVYDVLS   359
         ::.:.  **:    *****::****:*..*:********  *:*:*:* ***. ::*:***

                              |380
hACase   TKPVLNKLTVYTTLIDVTKGQFETYLRDCPDPCIGW                         395
Asah1a   TKPVLNKLTTYTSLMAVSTGTLESYVRDCPNPCTPW                         390
Asah1b   TKPVLNKLTTYYTTLMEVSKGTLESFIRDCPNPCMPW                        395
         *********.**:*: *:.* :*:::***:** *
```

Fig. 1. Alignment of the amino acid sequence of human ACase, zebrafish Asah1a, and Asah1b. The amino acid sequences of the precursor (prior to autocleavage) human ACase (Uniprot code Q13510), zebrafish Asah1a (Uniprot code Q5XJR7), and Asah1b (Uniprot code Q6PH71) are aligned using ClustalO(1.2.4) (45). (*) indicates a conserved residue between the three sequences, (:) indicates a strongly similar residue, and (.) indicates a more weak similar residue. The signal peptide is predicted using SignalP-5.0 and depicted in blue (44). Important residues in human ACase are colored: the catalytic Cys143 is depicted in red, Cys31-Cys340 forming a disulfide bridge in pink, residues important for substrate hydrolysis and autocleavage in orange (Arg159 and Asp162, Glu225, Asn320, and Arg332), and the four assigned glycosylation sites in green (31). ACase, acid ceramidase.

Only Asah1b generates GlcSph during GCase deficiency

To study the role of either ACase in generating GlcSph, we exposed developing zebrafish embryos lacking either Asah1a, Asah1b, or both, to ME656, a specific irreversible inhibitor of GCase (34). Inhibitor-treated WT zebrafish larvae (5 dpf) showed a significant increase in hexosylceramide (being primarily GlcCer (33)), GlcChol, and GlcSph (Fig. 3B, C). Contrary to Asah1a-deficient larvae, the GCase inhibitor-treated fish deficient in Asah1b did not develop the striking GlcSph elevation. These fish did show the accumulation of GlcCer and GlcChol (Fig. 3C). Likewise, GlcSph levels did not markedly increase in $gba1^{-/-}:asah1b^{-/-}$ larvae (supplemental Fig. S3). Thus, Asah1b is the principal enzyme responsible for the generation of excessive GlcSph during GCase deficiency. At present, we do not have information on the preference of Asha1b regarding particular GlcCer species. The vast majority of detected GlcSph has a 18:1 sphingoid base.

Farber fibroblasts stably overexpressing either human ACase, zebrafish Asah1a, or Asah1b showed a reduction of Cer (supplemental Fig. S4A). The finding substantiates that zebrafish Asah1a and Asah1b are the lysosomal homologs of human ACase. Next, we induced a GCase deficiency in these cells by exposure to a GCase specific inhibitor (34). In inhibitor-treated Farber fibroblasts, GlcSph is only formed in cells expressing Asah1b or human ACase and not those expressing Asah1a (supplemental Fig. S4B).

Gaucher-like cells in visceral organs of GCase-deficient zebrafish

WT, $gba1^{-/-}$, $asah1b^{-/-}$, and double deficient $gba1^{-/-}:asah1b^{-/-}$ fish were raised to adulthood. Relevant organs were examined at 12 wpf, by means of biochemistry and histopathology. Changes in swimming behavior and problems with feeding were already observed in some individual $gba1^{-/-}$ zebrafish starting around 10 or 11 wpf. These fish were therefore culled earlier when

Fig. 2. CRISPR/Cas9-mediated disruption of *asah1a* and *asah1b* in zebrafish. A: Top panel: Schematic representation of the *asah1a* gene on chromosome 14, encoding the predicted 390 amino acid Asah1a enzyme. Middle panel: DNA sequence of exon 3 of *asah1a* with sgRNA target 1 lined, the PAM site in red, and the protein sequence shown below. Lower panel: The 8 base pair deletion, as obtained from the sequence trace, would lead to a premature stopcodon (*). B: Top panel: Schematic representation of the *asah1b* gene on chromosome 4, encoding the predicted 395 amino acid Asah1b enzyme, with the exon in upper case and intron in lower case. Middle panel: DNA sequence of exon 4 of *asah1b* with sgRNA target 2 lined, the PAM site in red, and the protein sequence shown below. Lower panel: The sequence trace showed an insertion of 11 base pairs, which would lead to a change of amino acid sequence and a premature stopcodon (*).

predetermined humane endpoints were reached. We first focused on liver and spleen, organs prominently affected in GD patients (8). Relevant glycosphingolipids levels in liver tissue were determined by mass spectrometry. GlcSph was found to be significantly increased in the livers of $gba1^{-/-}$ fish but not of $gba1^{-/-}:asah1b^{-/-}$ fish (**Fig.** 4A). In contrast, hepatic GlcCer levels were increased comparably in $gba1^{-/-}$ and $gba1^{-/-}:asah1b^{-/-}$ fish. GlcChol was significantly increased in $gba1^{-/-}$ fish, but not in $gba1^{-/-}:asah1b^{-/-}$ fish.

Next, the livers were examined regarding the expression of specific mRNAs encoding specific proteins (Fig. 4B). A significant increase in expression of the storage-cell biomarker *gpnmb* was apparent in $gba1^{-/-}$ and $gba1^{-/-}:asah1b^{-/-}$ zebrafish livers pointing to the presence of GlcCer-laden macrophages. No prominent difference in the expression of an ortholog of human chitotriosidase (*chia.6*) was detected. Genes encoding the lysosomal protease Cathepsin D (*catD*) and the proinflammatory cytokine *il-1β* showed a slight, but not significant increase, while *tnfβ* (also known as tnf-α2 (48)) showed only a significant increase in $gba1^{-/-}$ livers.

Next, a histopathology examination was performed for which the whole body of the fish was sectioned in the sagittal plane to allow inspection of multiple organs and tissues (Fig. 4C–E). GlcCer-laden macrophages accumulate in the viscera of GD patients detected by light microscopy as enlarged foamy histocytes with a cell body resembling "crumpled tissue paper" (49, 50). Liver, pancreas, and spleen of $gba1^{-/-}$ and $gba1^{-/-}:asah1b^{-/-}$ showed multifocal presence of aggregates of foamy histiocytes (Fig. 4D, E). These Gaucher-like cells were not apparent in any of the WT or $asah1b^{-/-}$ fish (Figs. 4C and S5 for WT and $asah1b^{-/-}$, respectively). Overall, both $gba1^{-/-}$ fish, with Glcsph, and $gba1^{-/-}:asah1b^{-/-}$ without excessive GlcSph showed a massive increase in GlcCer in livers and presence of Gaucher-like cells in this organ, the likely source of the increased *gpnmb* transcript levels.

Persistent lipid abnormalities and inflammation in brains of both *gba1*- and *gba1:asah1b* KO fish

Next, brains of the generated mutant zebrafish were examined. Analysis of lipid levels revealed normal total Cer levels in $gba1^{-/-}:asah1b^{-/-}$ brains similar to WT, $gba1^{-/-}$, and $asah1b^{-/-}$ brains. Accumulation of GlcSph was profound in brains of $gba1^{-/-}$ zebrafish (from 0.16 to 130 pmol/mg for brains of WT and $gba1^{-/-}$, respectively), with no significant increase in brains of $gba1^{-/-}:asah1b^{-/-}$ fish (± 1.5 pmol/mg). The primary substrate of GCase, GlcCer, was comparably elevated in brains of both $gba1^{-/-}$ and $gba1^{-/-}:asah1b^{-/-}$ (± 100-fold and 120-fold). More modest abnormalities in other lipids were observed: the product glycosphingolipid LacCer was 22-
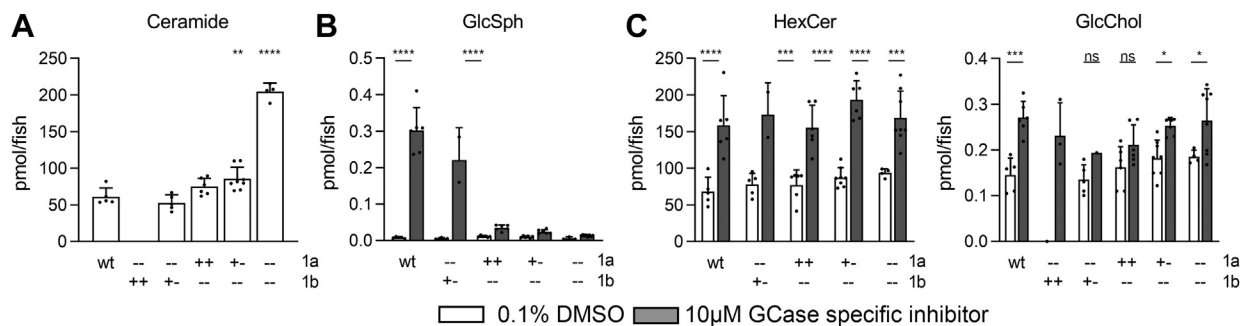
Fig. 3. (Glyco)sphingolipid abnormalities in Asah1a- and/or Asah1b-deficient zebrafish larvae. A: Total ceramide levels (pmol/fish) were determined of individual zebrafish larvae (5 dpf) of off-spring of $Asah1a^{+/-}:asah1b^{+/-}$ crossings. Data is depicted as mean ± SD and analyzed using a One-Way Anova with Dunnett's multiple comparisons Test and WT as control group. B: $Asah1a^{+/-}:asah1b^{+/-}$ adult zebrafish were crossed and off-spring was treated with vehicle (0.1% (v/v) DMSO) or 10 μm GCase specific inhibitor (ME656) for 5 days. Relevant lipid levels were determined of individual larvae in pmol/fish. WT (n = 5–6), $asah1a^{-}:asah1b^{+/-}$ (n = 1–5), $asah1a^{+/+}:asah1b^{-/-}$ (n = 6), $asah1^{+/-}:asah1b^{-/-}$ (n = 7–8), and $asah1a^{-/-}:asah1b^{-/-}$ (n = 4–8). Data is depicted as mean ± SD and analyzed using a Two-Way Anova with Sidak's multiple comparisons test. Ns = not significant, $*p < 0.05$, $**p < 0.01$, $***p < 0.001$, and $****p < 0.0001$.

fold and 33-fold elevated in brains of gba1$^{-/-}$ and gba1$^{-/-}$:asah1b$^{-/-}$ zebrafish, respectively. GlcChol was about 2.5-fold elevated in brains of gba1$^{-/-}$ zebrafish and 1.3-fold in brains of gba1$^{-/-}$:asah1b$^{-/-}$ zebrafish. The abundant myelin lipid GalCer was just slightly decreased in gba1$^{-/-}$ brains, however variation among individual fish in this lipid was marked.

Next, we analyzed and compared the expression of specific mRNAs in various brains. In both gba1$^{-/-}$ and gba1$^{-/-}$:asah1b$^{-/-}$ brains, expression of the GlcCer-laden macrophage markers, gpnmb and chia.6, was strikingly increased (± 70-fold for gpnmb and chia.6) (**Fig.** 5B). In parallel, we observed increased expression of mRNAs of the proinflammatory cytokines il1-β (± 10-fold and 13-fold for brains of gba1$^{-/-}$ and gba1$^{-/-}$:asah1b$^{-/-}$ fish, respectively) and tnfβ, also known as tnf-α2 (± 20-fold and 35-fold respectively) (Fig. 5B). In addition, increased catD mRNA expression (3-fold) and the microglia marker apoEb mRNA (5.5-7-fold) expression was detected in brains of both types of mutant fish lines. Activation of the complement system has previously been observed in GD mouse models, resulting in production of proinflammatory cytokines and chemokines (51). Expression of several genes encoding components of the complement system such as c1qA, c3.1, c5, and the c5a receptor (c5aR1) was significantly increased in brains of gba1$^{-/-}$ zebrafish. These genes were also markedly overexpressed in brains of gba1$^{-/-}$:asah1b$^{-/-}$ fish without GlcSph. Western blot analysis revealed an accumulation of the autophagy substrate p62 and an increase in the ratio of LC3-II to LC3-I in brains of both gba1$^{-/-}$ and gba1$^{-/-}$:asah1b$^{-/-}$ zebrafish, consistent with reduced autophagic flux due to the lysosomal phenotype (Fig. 5C, D). In conclusion, based on observed mRNA and protein levels of neuroinflammation, complement system activation and autophagy were found to be increased, but interestingly, no significant differences were found in any of the studied parameters between gba1 KOs accumulating GlcSph and gba1:asah1b KOs without excessive GlcSph.

The presence of Gaucher-like cells, detected by H&E staining, was evident in brains of both gba1$^{-/-}$ and gba1$^{-/-}$:asah1b$^{-/-}$ fish, but not in WT or asah1b$^{-/-}$ brains (**Figs.** 6A and S6). The Gaucher-like cells mainly accumulated in the periventricular gray zone of the optic tectum (Fig. 6A with zoom in Fig. 6B). Transverse sections of the midbrain showed severe diffuse bilateral accumulation of Gaucher-like cells filling the periventricular zone (Fig. 6C). Presence of Gaucher-like cells was confirmed by immunohistochemistry using the zebrafish monocyte/macrophage lineage cells marker L-plastin [42]. In addition we used immunostaining of L-plastin to visualize microglia activation (52). There was a marked increase in microglial cells in the brain parenchyma of gba1$^{-/-}$ and gba1$^{-/-}$:asah1b$^{-/-}$ zebrafish compared with controls (Figs. 6 and S6). In addition, microglia with swollen cell bodies were increased in the medulla oblongata of gba1$^{-/-}$ zebrafish and to a lesser extent in that of gba1$^{-/-}$:asah1b$^{-/-}$ fish (supplemental Fig. S6C). In conclusion, in brains of gba1$^{-/-}$ and gba1$^{-/-}$:asah1b$^{-/-}$ fish, a quite comparable presence of Gaucher-like cells was detected as well as comparable indicators of neuroinflammation, sharply contrasting to the marked difference in GlcSph levels between the two types of brains.

Next, loss of putative dopaminergic neurons in the various fish brains was assessed. For this, we determined the expression of mRNAs encoding tyrosine hydroxylase 1 (th1), a marker for dopaminergic neurons (42). This was reduced in gba1$^{-/-}$ zebrafish brains, while no significant reduction was observed in the gba1$^{-/-}$:asah1b$^{-/-}$ brains (Fig. 6E). The th2 mRNA expression was not abnormal. In addition, two transcripts of zebrafish orthologs of α-synuclein, sncβ, and sncγb were significantly reduced in gba1$^{-/-}$ brains compared to WT and gba1$^{-/-}$:asah1b$^{-/-}$ brains. The expression of myelin-binding protein (mbpa) was comparably reduced in both gba1$^{-/-}$ and asah1b$^{-/-}$:gba1$^{-/-}$ brains, suggesting disturbed myelination in both mutants. In conclusion, only significant differences were found in parameters related to putative dopaminergic neurons.
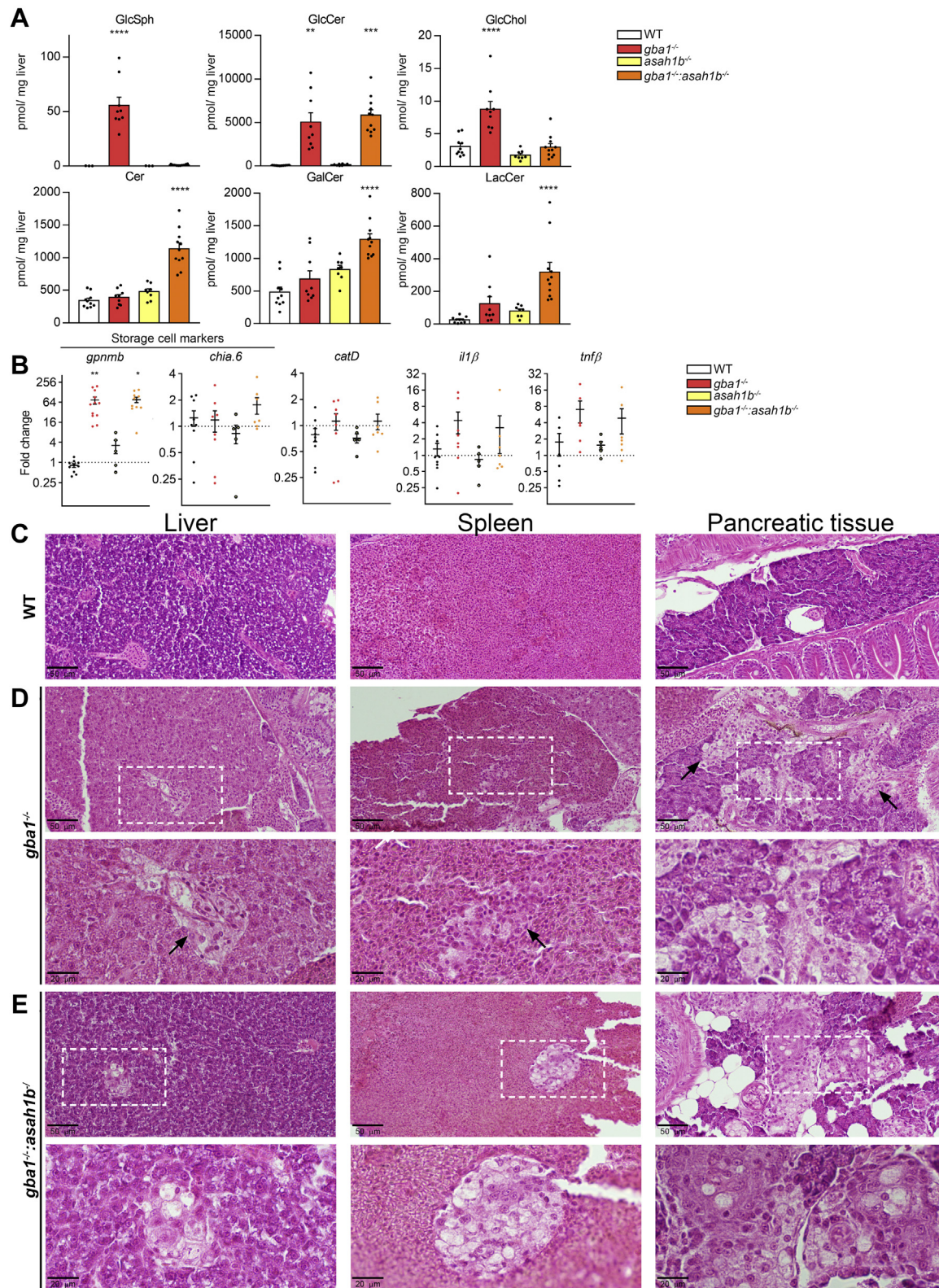
Fig. 4. Abnormalities in adult zebrafish visceral organs. A: Lipid levels were determined in pmol/mg liver tissue. GlcSph, GalCer, and GlcChol were separated from their respective galactosylated lipid by HILIC chromatography. Data is depicted as mean ± SEM; WT (n = 10), *gba1*^{-/-} (n = 9), *asah1b*^{-/-} (n = 8), and *gba1*^{-/-}:*asah1b*^{-/-} (n = 11). Data is analyzed by One-Way Anova with Tukey's multiple comparison test. B: Expression of *gpnmb, chia.6, il-1β, tnfβ, apoEb,* or *catD* mRNA levels were determined using RT-qPCR analysis; WT (n = 6–9), *gba1*^{-/-} (n = 6–8), *asah1b*^{-/-} (n = 5), and *gba1*^{-/-}:*asah1b*^{-/-} (n = 7). Data is normalized using two housekeeping genes (*ef1α* and *rpl13*) and analyzed by One-Way Anova with Tukey's multiple comparison test. Statistical analysis is depicted of WT versus *gba1*^{-/-}, *asah1b*^{-/-}, or *asah1b*:*gba1*^{-/-}, only when a significant difference is apparent or of *gba1*^{-/-} versus *asah1b*:*gba1*^{-/-} when significant difference is of interest. Ns = not significant, *$p < 0.05$,**$p < 0.01$, ***$p < 0.001$, and ****$p < 0.0001$. C–E, Zebrafish were serially sectioned along the
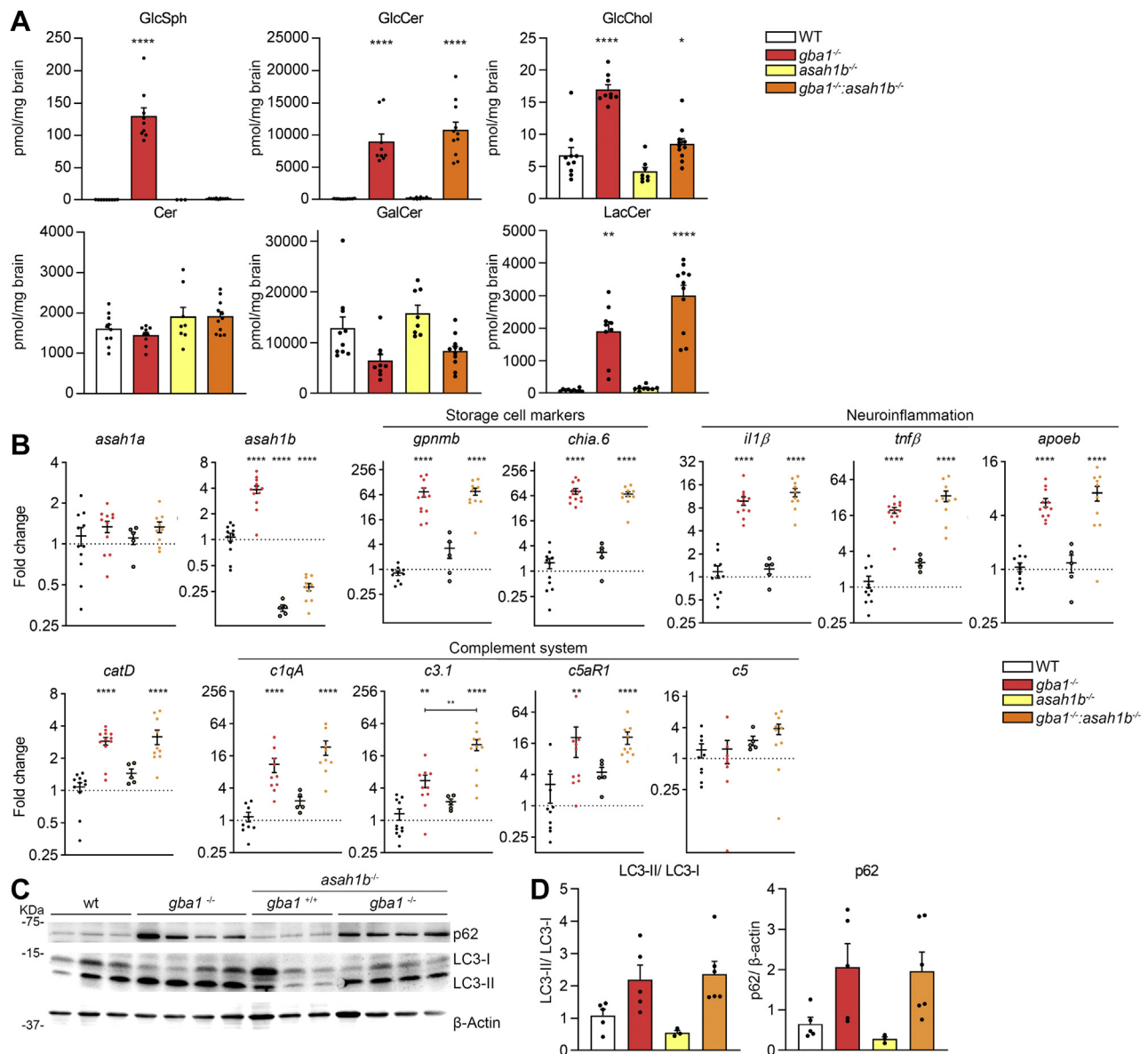
Fig. 5. Biochemical abnormalities in adult zebrafish brain. A: Lipid levels were determined of dissected brains in pmol/mg tissue. GlcSph, GalCer, and GlcChol were separated from their respective galactosylated lipid by HILIC chromatography. Data is depicted as mean ± SEM; WT (n = 9–10), $gba1^{-/-}$ (n = 9), $asah1b^{-/-}$ (n = 8), and $gba1^{-/-}:asah1b^{-/-}$ (n = 11). Data is analyzed by One-Way Anova with Tukey's multiple comparison test. B: mRNA levels of $asah1a$, $asah1b$, $gpnmb$, $chia.6$, $il-1\beta$, $tnf\beta$, $apoEb$, $catD$, $c1qA$, $c3.1$, $c5aR$, and $c5$ was determined using RT-qPCR analysis; WT (n = 9–11), $gba1^{-/-}$ (n = 8–11), $asah1b^{-/-}$ (n = 5), and $gba1^{-/-}:asah1b^{-/-}$ (n = 9–10). Data is analyzed by One-way Anova with Tukey's multiple comparison test. C: Representative Western blot of p62, LC3-I, LC3-II, β-catenin protein levels in WT, $gba1^{-/-}$, $asah1b^{-/-}$, and $gba1^{-/-}:asah1b^{-/-}$ zebrafish brains, with β-actin as protein loading control. D: Quantitative analysis of LC3-II/LC-I levels and p62 protein levels. WT (n = 5), $gba1^{-/-}$ (n = 5), $asah1b^{-/-}$ (n = 3), and $gba1^{-/-}:asah1b^{-/-}$ (n = 6). Statistical analysis is depicted of WT versus $gba1^{-/-}$, $asah1b^{-/-}$, or $asah1b^{-/-}:gba1^{-/-}$, only when a significant difference is apparent or of $gba1^{-/-}$ versus $asah1b:gba1^{-/-}$ when significant difference is of interest. *$p < 0.05$, **$p < 0.01$, and **** $p < 0.0001$. GalCer, galactosylceramide; GlcSph, glucosylsphingosine; GlcChol, glucosylated cholesterol.

Phenotypic improvements of adult Asah1b:Gba1 double KO zebrafish

Finally, we wondered if GlcSph impacts on the pathological phenotype of GCase-deficient zebrafish. No overt macroscopic phenotype was observed in any of the WT, $gba1^{-/-}$, $asah1b^{-/-}$, and $gba1^{-/-}:asah1b^{-/-}$ fish up to 8 wpf. From that age onwards, a hanging tail during rest became apparent in some of the $gba1^{-/-}$ zebrafish. Individual $gba1^{-/-}$ zebrafish with swimming abnormality had to be culled before the 12 wpf experimental

sagittal plane and stained using H&E. Images of liver, spleen, and pancreatic tissue of WT (C), $gba1^{-/-}$ (D), and $gba1^{-/-}:asah1b^{-/-}$ (E) zebrafish. Areas of interest are marked by dotted boxes, and higher magnifications of these areas are shown below the respective overview images. Scale bars: 50 μm and 20 μm for low and higher magnifications, respectively. GlcSph, glucosylsphingosine; GalCer, galactosylceramide; GlcChol, glucosylated cholesterol.
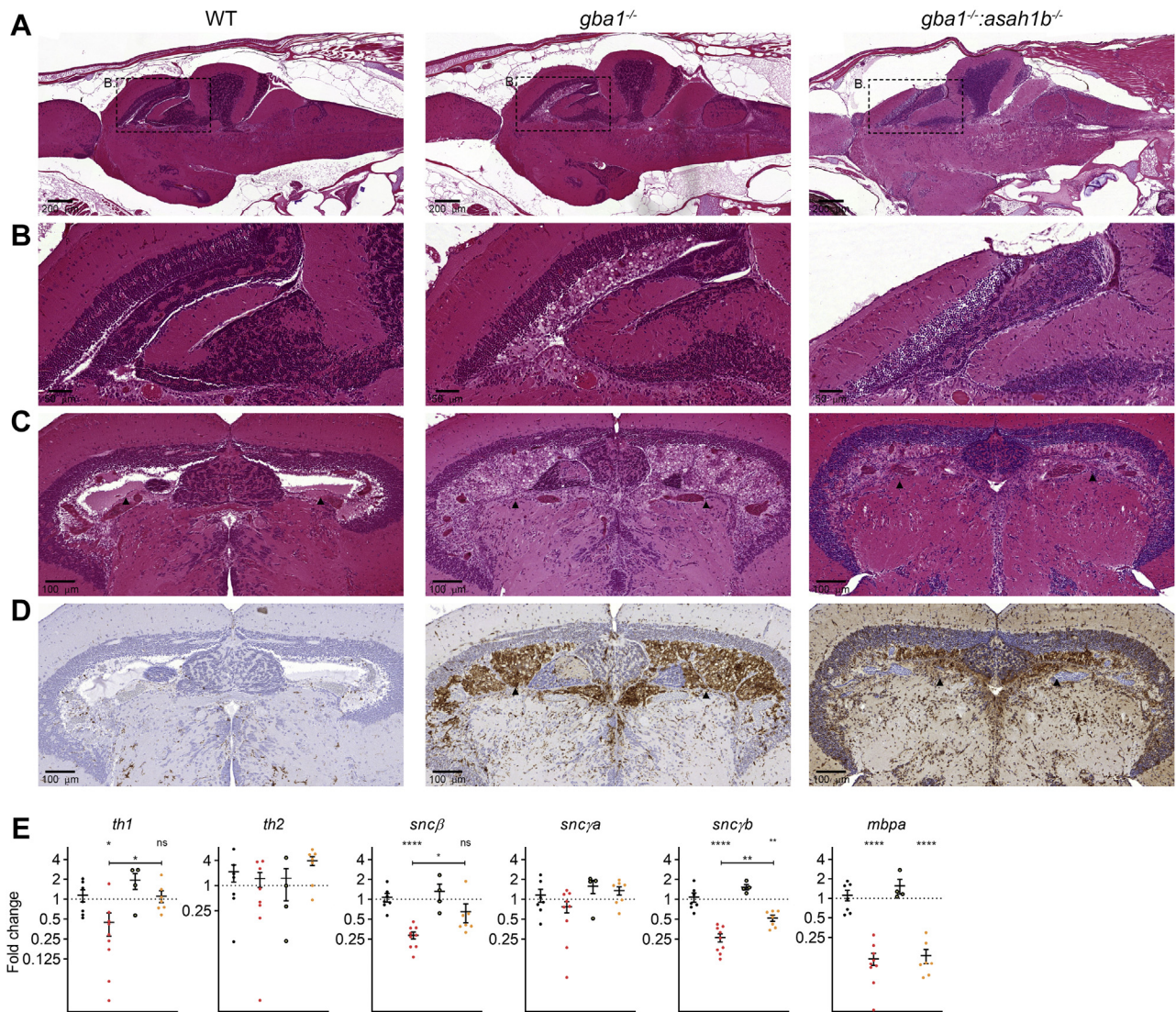
Fig. 6. Gaucher-like cells accumulate in *gba1⁻/⁻* and *gba1⁻/⁻:asah1b⁻/⁻* brains. A and B: WT, *gba1⁻/⁻*, and *gba1⁻/⁻:asah1b⁻/⁻* brains were serially sectioned in the sagittal plane and H&E stained. Gaucher-like cells occupy the periventricular zone of the optic tectum in both *gba1⁻/⁻I and gba1⁻/⁻:asah1b⁻/⁻* brain, with higher magnifications of the boxed areas in (A) and (B). Scale bars: 200 µm and 50 µm for the low and higher magnifications, respectively. C: Transverse view of WT, *gba1⁻/⁻*, and *gba1⁻/⁻:asah1b⁻/⁻* brains showing severe bilateral and diffuse accumulation of Gaucher-like cells in the periventricular gray zone of the optic tectum (HE). D: Immunohistochemistry for the zebrafish monocyte/macrophage lineage cells marker L-plastin. Immunoreactive macrophages were abundantly present in the ventricle and periventricular regions of *gba1⁻/⁻* and *gba1⁻/⁻:asah1b⁻/⁻* brains but not in the WT brain; counterstaining was performed using hematoxylin. Scale bars: 100 µm in C and D. E: mRNA expression of *th1, th2, sncβ, sncγa, sncγb*, and *mbpa* was determined using RT-qPCR analysis; WT (n = 7), *gba1⁻/⁻* (n = 9), *asah1b⁻/⁻* (n = 4), and *gba1⁻/⁻:asah1b⁻/⁻* (n = 7). Data of RT-qPCR is normalized using two housekeeping genes (*ef1α* and *rpl13*), analyzed by One-Way Anova with Tukey's multiple comparisons test or a Brown-Forsythe and Welch Anova with Dunnett's multiple comparisons test for *gpnmb* and *chia.6* and depicted as scattered dot plot ± SEM. Statistical analysis is depicted of WT versus *gba1⁻/⁻*, *asah1b⁻/⁻*, or *asah1b⁻/⁻:gba1⁻/⁻*, only when a significant difference is apparent or of *gba1⁻/⁻* versus *asah1b:gba1⁻/⁻* when significant difference is of interest. Ns = not significant, *$p < 0.05$, **$p < 0.01$, and ****$p < 0.0001$.

endpoint. Differences were noticeable among the different types of mutant fish as well as variation among individual fish within each genotype. All *gba1⁻/⁻* zebrafish (t= 10–12 wpf) showed phenotypic abnormalities such as a curved back and different swimming behavior compared to WT (**Fig. 7**A and supplemental Videos S1 and S2; red stickers). The morphology of the various fish was compared by measurement of the body length and curvature of the back, assessed by dividing the length of the back by the body length

(tortuosity). The body length of the *gba1⁻/⁻* zebrafish was significant smaller than WT, while the tortuosity was significantly enlarged (Fig. 7B). Most of the *gba1⁻/⁻* zebrafish showed abnormal swimming behavior, ranging from difficulty with balance, failure to maintain an upright position to the inability to move from the bottom of the tank (supplemental Videos S1 and S2). In order to analyze and compare their behavior, individual zebrafish were tracked and their swimming speed and time spend in the upper part of the tank was
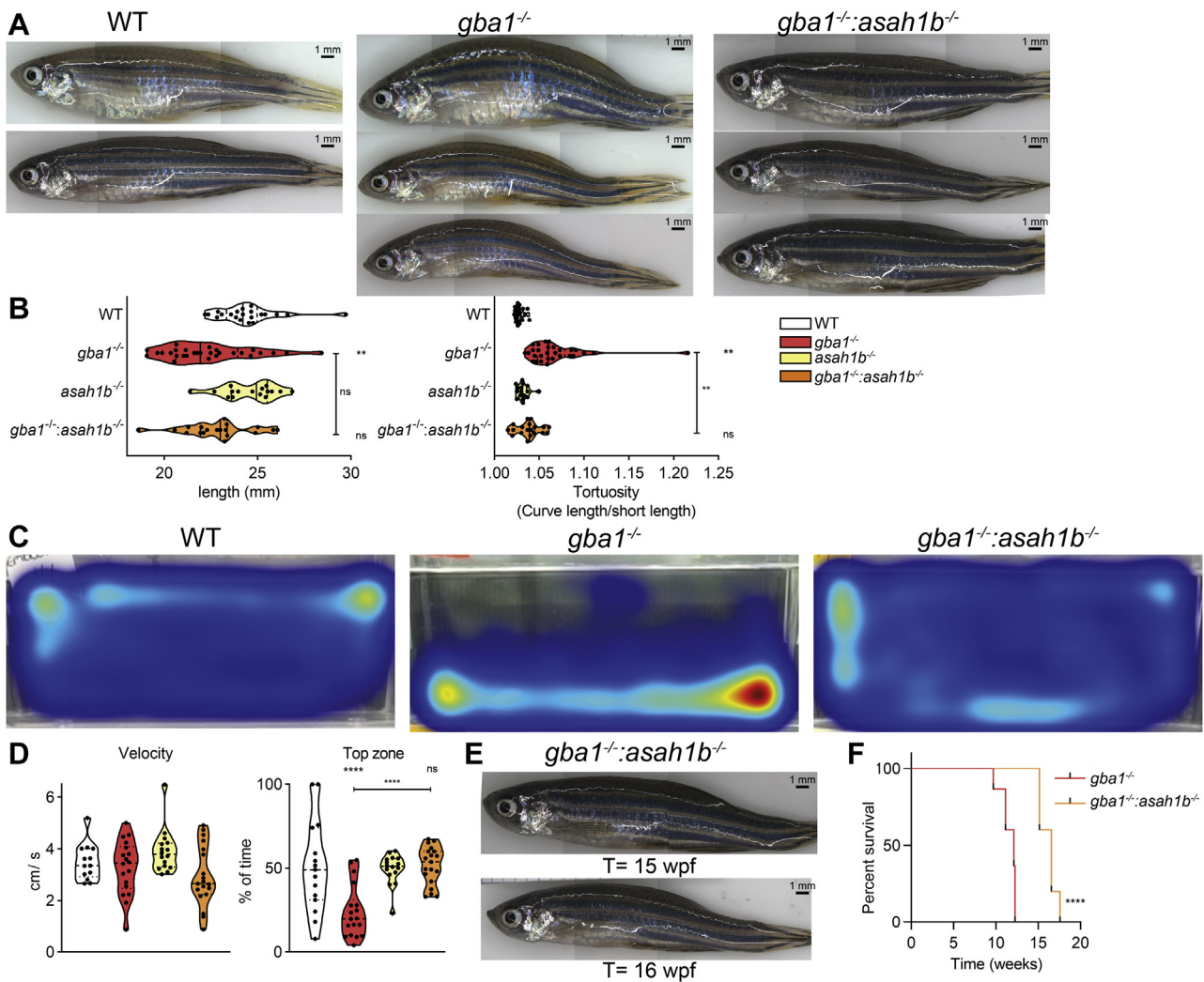
Fig. 7. Phenotypic improvements of adult Asah1b:Gba1 double deficient zebrafish. A: Representative photographs of WT, *gba1*⁻/⁻, and *gba1*⁻/⁻:*asah1b*⁻/⁻ zebrafish. B: The length of individual zebrafish is determined (head to tail base) as well as the tortuosity, calculated as ratio of the length along the back divided by the length of the fish, as indication for the curved back. Data of individual zebrafish is depicted in a violin plot; WT (n = 21), *gba1*⁻/⁻ (n = 29), *asah1b*⁻/⁻ (n = 16), and *gba1*⁻/⁻:*asah1b*⁻/⁻ (n = 19) and analyzed using a nonparametric Kruskal–Wallis test with Dunn's multiple comparison test. C: Representative movement traces of WT, *gba1*⁻/⁻, and *gba1*⁻/⁻:*asah1b*⁻/⁻ zebrafish, all at t = 12 wpf. D: Quantification of individual zebrafish average velocity (in cm/s) when in motion and time spend in the top half of the tank. Data of individual zebrafish is depicted in a violin plot; WT (n = 13), *gba1*⁻/⁻ (n = 16), *asah1b*⁻/⁻ (n = 16), and *gba1*⁻/⁻:*asah1b*⁻/⁻ (n = 19) and analyzed using a One-Way Anova with Tukey's multiple comparison test. E: Photograph of individual *gba1*⁻/⁻:*asah1b*⁻/⁻ zebrafish at t = 15 and 16 wpf. F: Kaplan-Meier plot indicating the onset of predetermined symptoms, such as the curved back and abnormal swimming resulting in impaired feeding behavior, of *gba1*⁻/⁻ and *gba1*⁻/⁻:*asah1b*⁻/⁻ zebrafish; *gba1*⁻/⁻ (n = 30), and *gba1*⁻/⁻:*asah1b*⁻/⁻ (n = 5). The curves are analyzed using a Log-rank (Mantel-Cos) test. Statistical analysis is depicted of WT versus *gba1*⁻/⁻, *asah1b*⁻/⁻ or *asah1b*⁻/⁻:*gba1*⁻/⁻, only when a significant difference is apparent or of *gba1*⁻/⁻ versus *asah1b:gba1*⁻/⁻ when significant difference is of interest. Ns = not significant, **$p < 0.01$ and ****$p < 0.0001$. wpf, week postfertilization.

quantified (Fig. 7C, D). The average velocity of the *gba1*⁻/⁻ zebrafish in motion was not significantly different (Fig. 7D), and no difference in average angular velocity was found either (data not shown). A significant difference was observed in the ability of the zebrafish to use the entire space of the tank. In contrast to WT fish, *gba1*⁻/⁻ zebrafish spent significantly less time in the top of the tank (Fig. 7C, D).

Of note, contrary to *gba1*⁻/⁻ fish, none of the *gba1*⁻/⁻:*asah1b*⁻/⁻ fish showed a significant difference in length or tortuosity at 12 wpf (Fig. 7A, B). Additionally, *gba1*⁻/⁻:*asah1b*⁻/⁻ did not show postural imbalance and

used the whole tank for swimming as also observed for WT and *asah1b*⁻/⁻ zebrafish (Fig. 7C, D, supplemental Videos S1–S3; orange stickers for *gba1*⁻/⁻:*asah1b*⁻/⁻). Therefore, we performed a longevity study by raising the *gba1*⁻/⁻:*asah1b*⁻/⁻ zebrafish past 12 wpf until similar phenotypic abnormalities became apparent as those of g*ba1*⁻/⁻ zebrafish at 10 to 12 wpf. Individual double mutant zebrafish started showing the phenotypic abnormalities, such as a curved back, postural imbalance, and abnormal swimming behavior at around 15–17 wpf (Figs. 7E and S7). Thus, there was a marked amelioration of disease course in the *gba1*⁻/⁻:*asah1b*⁻/⁻

zebrafish lacking excessive GlcSph. The lifespan of all $gba1^{-/-}$:$asah1b^{-/-}$ zebrafish was increased, some even by 7 weeks, almost a doubling (Fig. 7F). Importantly, the absence of GlcSph did not prevent on the longer run phenotypic abnormalities such as the curved back and differences in swimming behavior.

DISCUSSION

Our investigation has profited from the fortuitous duplication of the *asah1* gene that occurred in zebrafish, coupled to the evolution of an apparent different substrate specificity of the Asah1a and Asah1b orthologs. Both fish ACases hydrolyze its primary substrate Cer, but only Asah1b proves to be involved in formation of GlcSph during GCase deficiency. This fact allowed us to compare adult $gba1^{-/-}$ (GD) fish with excessive GlcSph with those without this lyso-lipid ($gba1^{-/-}$:$asah1b^{-/-}$ GD fish). Both types of GD fish show comparable prominent accumulation of Gaucher-like cells in tissues, similar as observed in animal models of GD and patients (41, 43, 53). Thus, it appears that the ACase–mediated GlcSph formation only marginally reduces GlcCer accumulation during GCase deficiency in macrophages of zebrafish.

It is tempting to compare the outcome of GCase deficiency in fish producing GlcSph from accumulating GlcCer in lysosomes ($gba1^{-/-}$ GD fish) with those that cannot ($gba1^{-/-}$:$asah1b^{-/-}$ GD fish). Clearly, prevention of GlcSph formation does not result in a worse disease in the GD zebrafish. Apparently, only a fraction of accumulating GlcCer is converted to GlcSph and may subsequently leave the body via urine or bile. Thus, formation and subsequent excretion of GlcSph offers no prevention of the formation of lipid-laden storage cells. The GD fish with excessive GlcSph and those without show similar amounts of Gaucher-like storage cells in tissues and similar markers of neuroinflammation, increased autophagy, and complement cascade activation in the brain. Thus, the chronic presence of GlcSph does not appear to markedly promote one of these pathophysiological processes. On the other hand, the clinical course of $gba1^{-/-}$:$asah1b^{-/-}$ GD fish lacking GlcSph seems more benign as that of $gba1^{-/-}$ GD fish. This is best reflected in a slower development of a permanently curved back and swimming abnormalities as well as increased lifespan of $gba1^{-/-}$:$asah1b^{-/-}$ GD fish lacking GlcSph. However, ultimately, these animals do develop the same phenotypic abnormalities as $gba1^{-/-}$ GD fish. As shown in supplemental Fig. S8, inspection of spinal cords of WT, $gba1^{-/-}$, and $gba1^{-/-}$:$asah1b^{-/-}$ fish revealed no overt abnormalities. Earlier Zhou et al. (36) reported that a morpholino knockdown of *asah1b* led to an abnormal spinal cord of *Danio* embryos. We have no explanation for this discrepancy. Possibly, different methodology (morpholino knockdown and CRISPR-Cas ablation of asah1b) offers an explanation.

The observations above appear conflicting with presently popular ideas on a dominant acute toxicity of lysolipids like glucosylsphingosine as well as a dominant acute toxicity of storage cells and neuroinflammation (54). Therefore, both topics warrant further consideration and discussion. Firstly, the apparent absence of acute toxicity of GlcSph to many cells in the viscera. Histological examination suggests that many cell types in viscera tolerate the chronic presence of GlcSph amazingly well. In fact, a similar notion is obtained from GD patients in which many cell types do well despite the high circulating and tissue GlcSph levels (15). Acute dysfunction of mitochondria or key enzymes by direct inhibition by GlcSph seems therefore not a likely scenario: cells might get stressed but clearly can still thrive. However, as discussed in more detail below, dopaminergic neurons may be particular vulnerable in this aspect. The second surprising observation concerns the limited impact of chronic high GlcSph and incidence of storage cells on inflammation in combination with the observed improvement in phenotype of fish lacking excessive GlcSph. In fact, the cumulative research by Futerman et al. in neuronopathic GD (nGD) mice have presented evidence that inflammation, contrary to earlier considerations (54), is not the dominant determinant of neurotoxicity in GD (55, 56). For example, the IFN pathway is prominently activated in the brain of nGD mice. The ablation of upstream pathways leading to IFN production had no therapeutic benefit on the lifespan of nGD mice but attenuated neuroinflammation (55). Our findings are consistent with this notion by Futerman et al., at least in GBA1 deficient brains, neuroinflammation is not entirely dependent on GlcSph and neuroinflammation is not synonymous with some neurological signs such as locomotor abnormality and development of an abnormal curved back posture.

The apparent impact of excessive GlcSph on GCase-deficient putative dopaminergic neurons warrants discussion. Interestingly, the expression of mRNAs encoding tyrosine hydroxylase 1 (*th1*), a marker for dopaminergic neurons, is reduced in $gba1^{-/-}$ zebrafish brains, but not $gba1^{-/-}$:$asah1b^{-/-}$ brains. Zebrafish β-synuclein and γ1-synuclein (*sncγb* gene) isoforms are expressed in the cell bodies of TH-positive catecholaminergic cells (57). An ortholog of human α-synuclein is not present in the zebrafish genome (57). In our experiments, the two transcripts of zebrafish synucleins, *sncβ* and *sncγb*, were significantly reduced in *gba1* KO brains compared to WT and *gba1:asah1b* KO brains, while the expression of myelin-basic protein (*mbpa*) was comparably reduced in both mutant brains. Keatinge et al. (43) observed a reduction of TH-immunoreactive neurons in the caudal hypothalamus and posterior tuberculum and a reduction of β- and γ1-synuclein proteins in $gba1^{-/-}$ zebrafish. Thus, our earlier findings suggest that increased GlcSph negatively impacts on TH-positive dopaminergic neurons.

Other observations also have pointed to a detrimental role of excessive GlcSph regarding dopaminergic neurons. In neuronopathic GD/PD mouse models, GlcCer was found to be not increased in the brain while GlcSph accumulation already occurred in young mice (8–12 weeks), supposedly somehow triggering α-synuclein aggregation as observed with cultured human neuronal cells (18). In addition, a recent study with mice heterozygous for GCase deficiency showed development of α-synucleinopathy concomitant to overproduction of GlcSph (17). The absence of α-synuclein in zebrafish, and the different location of dopaminergic neurons as compared to human brain, limits the use as genuine Parkinson's disease model. Of note, *Oryzias latipes* (medaka) fish do express α-synuclein (58). Another recent elegant study corroborates the toxicity of GlcSph regarding dopaminergic neurons. Feldman et al. (59) studied human-induced pluripotent stem cell-derived neurons from neurologically affected GD patients. Elevated levels of GlcSph in these cells were found to activate mammalian target of rapamycin (mTOR) complex 1, interfering with lysosomal biogenesis and autophagy. Inhibition of ACase prevented both, mTOR hyperactivity and lysosomal dysfunction, suggesting that these alterations were caused by GlcSph accumulation in the mutant neurons. Incubation of WT neurons with exogenous GlcSph was also found to induce the harmful mTOR hyperactivation.

Our study focused primarily on the impact of GlcSph on presence of lipid-laden macrophages in tissues. The neuropathological aspects of $gba1^{-/-}$ zebrafish are more completely documented by Keatinge et al. (43). We studied general swimming of individual adult fish and noticed clear differences in $gba1^{-/-}$ fish, not using the whole tank. More advanced methods are available to study behavioral defects, including learning and social interaction assays as reviewed by Vaz et al. (60). Although zebrafish are an increasingly popular model to study mechanisms underlying Parkinson's disease, also in connection to increased risk posed by mutations in the *GBA1* allele (GD-PD), it might not offer a straightforward model for human GD-PD. Firstly, we generated zebrafish with a complete loss in GCase (activity). Others employing GCase suicide inhibitors generate animals with a complete loss of enzymatic activity. Both conditions markedly differ from human GD-PD in which patients have a significant residual GCase (7). In fact, the $gba1^{-/-}$ fish are also not a true model of the most common phenotypes of GD with residual enzyme. Furthermore, there are intrinsic differences between humans and zebrafish in key molecular players in PD, such as the absence of α-synuclein in the latter species. In fact, the relationship between the *GBA1* locus and the risk for PD is still largely elusive (7). Only a fraction of carriers of mutant *GBA1* alleles, largely independent of the severity of the underlying mutations, develop PD. To complicate matters further, it has been reported that deficiency of GCase in dopaminergic neurons themselves does not lead to an increased risk for PD symptoms in mice (61). Therefore, simply translating the findings made in our present study to human GD-PD is not wise, and over-interpreting findings in zebrafish models to human disease should be avoided.

At present, it remains unclear whether excessive GlcSph itself drives putative dopaminergic neuronal loss or whether microglia activation, likely driven by GlcCer accumulation and lysosomal dysfunction assists the neurodegeneration. Conceivably, both processes might occur hand in hand to a variable extent. Of interest, the consequences of pharmacologically induced GCase deficiency in different mice strains with conduritol B-epoxide may differ dramatically (62). It was observed that the age of survival following conduritol B-epoxide administration varied from 40–200 days (62). It is important to point out that despite the delayed disease manifestations and improved lifespan, *gba1:asah1b* KO fish lacking GlcSph still develop abnormal swimming behavior at 4 months of age and need to be culled earlier than WT and *asah1b* single KO zebrafish. This suggests that GlcSph contributes significantly to the onset of GD symptoms, but it is not the only pathogenic factor. In this respect, the impact of specific accumulating GlcCer species and other glucosylated lipids such as GlcChol (38) deserves further attention. Future studies with Gba2 KO GD fish, unable to produce GlcChol, should provide insight on a possible contribution of the glycosylated sterol in GD pathology. In theory, the introduction of Asah1b deficiency in $gba1^{-/-}$ fish might lead to other lipid abnormalities beyond the reduction in GlcSph. We did not observe prominent lipid abnormalities in $asah1b^{-/-}$ fish . In the $gba1^{-/-}:asah1b^{-/-}$ fish, slightly increased hepatic levels of Cer, GalCer, and LacCer, and increased LacCer and decreased GlcChol were observed. Likely, these minor abnormalities stem partly from the presence of storage cells in the tissues of GCase-deficient fish and do not contribute to the more benign clinical course of the $gba1^{-/-}:asah1b^{-/-}$ fish.

Inhibition of ACase is considered as therapeutic avenue in neuronopathic GD with unmet need. Carmofur is a known inhibitor of ACase (63, 64). It has been earlier demonstrated that Carmofur treatment of GCase-deficient cells reduces formation of GlcSph (24). The compound Carmofur is however not a specific ACase inhibitor, as it also inactivates neutral ceramidases and it is known to inhibit the nucleotide-synthesizing enzyme thymidylate synthetase, an effect underlying its wide-spread use as chemotherapeutic agent (63). More specific ACase inhibitors have been designed by Fabrias et al. (65). The window for such type of intervention might be very small, or even not exist, given the report that partial ACase deficiency already impairs spinal-cord motor neurons and other areas of the CNS (66).

The ACase-mediated formation of deacylated sphingolipid bases is not unique to GD. A similar phenomenon is observed with other lysosomal sphingolipidoses: Fabry disease with globotriaosylsphingosine (lysoGb3) formed from accumulating globotriaosylceramide (Gb3); Krabbe disease with galactosylsphingosine (GalSph) formed from GalCer; acid sphingomyelinase deficiency, a.k.a. Niemann-Pick disease types A and B, with phosphocholine-sphingosine (lysosphingomyelin) formed from sphingomyelin (67, 68). As for GlcSph in GD disease, toxic actions of lysoGb3 in Fabry disease and GalSph in Krabbe disease have been studied (69–72). Recently, ablation of ACase in a mouse model of Krabbe disease deficient in galactocerebrosidase (GALC) was found to prevent GalSph accumulation in brain, liver, and spleen tissue (69). A reduction of activated macrophages/microglia in the cerebellum, improved axonal structures, fewer infiltrating inflammatory cells, less edema, improved motor activity, and increased lifespan were observed compared to GALC-only deficient mice. On the other hand, increased levels of Cer were apparent in the liver and spleen of the GALC/ACase-deficient mice as well as hematological abnormalities such as vacuoles in the spleen, circulating monocyte, and neutrophil populations, as observed in the ACase-deficient mice (69). As opposed to the mice models, our Asah1b-deficient zebrafish without Cer accumulation could offer interesting opportunities to investigate the detrimental role of deacylated sphingolipid bases in the outcome of other lysosomal storage diseases, without the accompanying Cer accumulation.

In conclusion, our investigation of GCase-deficient zebrafish with or without concomitant deficiency of Asah1b provides evidence that inability to form GlcSph ($asah1b^{-/-}$) does not worsen disease, suggesting that excretion of water-soluble GlcSph is not an effective protection against symptoms. Lack of excessive GlcSph increases lifespan and seems to slow down the loss of dopaminergic neurons as revealed by *th1* mRNA. However, even in the absence of excessive lyso-lipid, $gba1^{-/-}:asah1b^{-/-}$ fish ultimately develop fatal pathology. Thus, GlcSph seems not to be the sole player in the pathophysiology during GCase deficiency in zebrafish.

Data availability

The data supporting this study are included in the published article and its supplemental data. 🔲

Author ORCIDs

Lindsey T. Lelieveld https://orcid.org/0000-0001-5584-7266
Marta Artola https://orcid.org/0000-0002-3051-3902
Annemarie H. Meijer https://orcid.org/0000-0002-1325-0725
Rolf G. Boot https://orcid.org/0000-0002-7031-3390

REFERENCES

1. Ferraz, M. J., Kallemeijn, W. W., Mirzaian, M., Herrera Moro, D., Marques, A., Wisse, P., Boot, R. G., Willems, L. I., Overkleeft, H. S., and Aerts, J. M. (2014) Gaucher disease and Fabry disease: new markers and insights in pathophysiology for two distinct glycosphingolipidoses. *Biochim. Biophys. Acta.* **1841**, 811–825
2. Bodamer, O. A., and Hung, C. (2010) Laboratory and genetic evaluation of Gaucher disease. *Wien Med. Wochenschr.* **160**, 600–604
3. Mechtler, T. P., Stary, S., Metz, T. F., De Jesus, V. R., Greber-Platzer, S., Pollak, A., Herkner, K. R., Streubel, B., and Kasper, D. C. (2012) Neonatal screening for lysosomal storage disorders: feasibility and incidence from a nationwide study in Austria. *Lancet.* **379**, 335–341
4. Pollak, A., and Kasper, D. C. (2014) Austrian newborn screening program: a perspective of five decades. *J. Perinat. Med.* **42**, 151–158
5. Platt, F. M., d'Azzo, A., Davidson, B. L., Neufeld, E. F., and Tifft, C. J. (2018) Lysosomal storage diseases. *Nat. Rev. Dis. Primers.* **4**, 27
6. Sidransky, E., Nalls, M. A., Aasly, J. O., Aharon-Peretz, J., Annesi, G., Barbosa, E. R., Bar-Shira, A., Berg, D., Bras, J., Brice, A., Chen, C. M., Clark, L. N., Condroyer, C., De Marco, E. V., Durr, A., *et al.* (2009) Multicenter analysis of glucocerebrosidase mutations in Parkinson's disease. *N. Engl. J. Med.* **361**, 1651–1661
7. Do, J., McKinney, C., Sharma, P., and Sidransky, E. (2019) Glucocerebrosidase and its relevance to Parkinson disease. *Mol. Neurodegener.* **14**, 36

8. Beutler, E., and Grabowski, G. A. (2001) Gaucher disease. In *The Metabolic and Molecular Bases of Inherited Disease*. C. R. Scriver, A. L. Beaudet, W. S. Sly, and D. Valle, editors. McGraw-Hill, New York, 3635–3668

9. Hollak, C. E., van Weely, S., van Oers, M. H., and Aerts, J. M. (1994) Marked elevation of plasma chitotriosidase activity. A novel hallmark of Gaucher disease. *J. Clin. Invest.* **93**, 1288–1292

10. Boot, R. G., Verhoek, M., de Fost, M., Hollak, C. E., Maas, M., Bleijlevens, B., van Breemen, M. J., van Meurs, M., Boven, L. A., Laman, J. D., Moran, M. T., Cox, T. M., and Aerts, J. M. (2004) Marked elevation of the chemokine CCL18/PARC in Gaucher disease: a novel surrogate marker for assessing therapeutic intervention. *Blood.* **103**, 33–39

11. Kramer, G., Wegdam, W., Donker-Koopman, W., Ottenhoff, R., Gaspar, P., Verhoek, M., Nelson, J., Gabriel, T., Kallemeijn, W., Boot, R. G., Laman, J. D., Vissers, J. P., Cox, T., Pavlova, E., Moran, M. T., *et al.* (2016) Elevation of glycoprotein nonmetastatic melanoma protein B in type 1 Gaucher disease patients and mouse models. *FEBS Open Bio.* **6**, 902–913

12. van Dussen, L., Hendriks, E. J., Groener, J. E., Boot, R. G., Hollak, C. E., and Aerts, J. M. (2014) Value of plasma chitotriosidase to assess non-neuronopathic Gaucher disease severity and progression in the era of enzyme replacement therapy. *J. Inherit. Metab. Dis.* **37**, 991–1001

13. Deegan, P. B., Moran, M. T., McFarlane, I., Schofield, J. P., Boot, R. G., Aerts, J. M., and Cox, T. M. (2005) Clinical evaluation of chemokine and enzymatic biomarkers of Gaucher disease. *Blood Cells Mol. Dis.* **35**, 259–267

14. Murugesan, V., Liu, J., Yang, R., Lin, H., Lischuk, A., Pastores, G., Zhang, X., Chuang, W. L., and Mistry, P. K. (2018) Validating glycoprotein non-metastatic melanoma B (gpNMB, osteoactivin), a new biomarker of Gaucher disease. *Blood Cells Mol. Dis.* **68**, 47–53

15. Dekker, N., van Dussen, L., Hollak, C. E., Overkleeft, H., Scheij, S., Ghauharali, K., van Breemen, M. J., Ferraz, M. J., Groener, J. E., Maas, M., Wijburg, F. A., Speijer, D., Tylki-Szymanska, A., Mistry, P. K., Boot, R. G., *et al.* (2011) Elevated plasma glucosylsphingosine in Gaucher disease: relation to phenotype, storage cell markers, and therapeutic response. *Blood.* **118**, e118–e127

16. Nair, S., Boddupalli, C. S., Verma, R., Liu, J., Yang, R., Pastores, G. M., Mistry, P. K., and Dhodapkar, M. V. (2015) Type II NKT-TFH cells against Gaucher lipids regulate B-cell immunity and inflammation. *Blood.* **125**, 1256–1271

17. Ikuno, M., Yamakado, H., Akiyama, H., Parajuli, L. K., Taguchi, K., Hara, J., Uemura, N., Hatanaka, Y., Higaki, K., Ohno, K., Tanaka, M., Koike, M., Hirabayashi, Y., and Takahashi, R. (2019) GBA haploinsufficiency accelerates alpha-synuclein pathology with altered lipid metabolism in a prodromal model of Parkinson's disease. *Hum. Mol. Genet.* **28**, 1894–1904

18. Taguchi, Y. V., Liu, J., Ruan, J., Pacheco, J., Zhang, X., Abbasi, J., Keutzer, J., Mistry, P. K., and Chandra, S. S. (2017) Glucosylsphingosine promotes alpha-synuclein pathology in mutant GBA-associated Parkinson's disease. *J. Neurosci.* **37**, 9617–9631

19. Reed, M. C., Schiffer, C., Heales, S., Mehta, A. B., and Hughes, D. A. (2018) Impact of sphingolipids on osteoblast and osteoclast activity in Gaucher disease. *Mol. Genet. Metab.* **124**, 278–286

20. Smith, N. J., Fuller, M., Saville, J. T., and Cox, T. M. (2018) Reduced cerebral vascularization in experimental neuronopathic Gaucher disease. *J. Pathol.* **244**, 120–128

21. Lukas, J., Cozma, C., Yang, F., Kramp, G., Meyer, A., Nesslauer, A. M., Eichler, S., Bottcher, T., Witt, M., Brauer, A. U., Kropp, P., and Rolfs, A. (2017) Glucosylsphingosine causes hematological and visceral changes in mice-evidence for a pathophysiological role in Gaucher disease. *Int. J. Mol. Sci.* **18**, 2192

22. Dahl, M., Doyle, A., Olsson, K., Mansson, J. E., Marques, A. R. A., Mirzaian, M., Aerts, J. M., Ehinger, M., Rothe, M., Modlich, U., Schambach, A., and Karlsson, S. (2015) Lentiviral gene therapy using cellular promoters cures type 1 Gaucher disease in mice. *Mol. Ther.* **23**, 835–844

23. Dekker, N., Voorn-Brouwer, T., Verhoek, M., Wennekes, T., Narayan, R. S., Speijer, D., Hollak, C. E., Overkleeft, H. S., Boot, R. G., and Aerts, J. M. (2011) The cytosolic beta-glucosidase GBA3 does not influence type 1 Gaucher disease manifestation. *Blood Cells Mol. Dis.* **46**, 19–26

24. Ferraz, M. J., Marques, A. R., Appelman, M. D., Verhoek, M., Strijland, A., Mirzaian, M., Scheij, S., Ouairy, C. M., Lahav, D., Wisse, P., Overkleeft, H. S., Boot, R. G., and Aerts, J. M. (2016) Lysosomal glycosphingolipid catabolism by acid ceramidase: formation of glycosphingoid bases during deficiency of glycosidases. *FEBS Lett.* **590**, 716–725

25. Yamaguchi, Y., Sasagasako, N., Goto, I., and Kobayashi, T. (1994) The synthetic pathway for glucosylsphingosine in cultured fibroblasts. *J. Biochem.* **116**, 704–710

26. Park, J. H., and Schuchman, E. H. (2006) Acid ceramidase and human disease. *Biochim. Biophys. Acta.* **1758**, 2133–2138

27. Yu, F. P. S., Amintas, S., Levade, T., and Medin, J. A. (2018) Acid ceramidase deficiency: farber disease and SMA-PME. *Orphanet J. Rare Dis.* **13**, 121

28. Okino, N., He, X., Gatt, S., Sandhoff, K., Ito, M., and Schuchman, E. H. (2003) The reverse activity of human acid ceramidase. *J. Biol. Chem.* **278**, 29948–29953

29. Bernardo, K., Hurwitz, R., Zenk, T., Desnick, R. J., Ferlinz, K., Schuchman, E. H., and Sandhoff, K. (1995) Purification, characterization, and biosynthesis of human acid ceramidase. *J. Biol. Chem.* **270**, 11098–11102

30. Ferlinz, K., Kopal, G., Bernardo, K., Linke, T., Bar, J., Breiden, B., Neumann, U., Lang, F., Schuchman, E. H., and Sandhoff, K. (2001) Human acid ceramidase: processing, glycosylation, and lysosomal targeting. *J. Biol. Chem.* **276**, 35352–35360

31. Gebai, A., Gorelik, A., Li, Z., Illes, K., and Nagar, B. (2018) Structural basis for the activation of acid ceramidase. *Nat. Commun.* **9**, 1621

32. Dementiev, A., Joachimiak, A., Nguyen, H., Gorelik, A., Illes, K., Shabani, S., Gelsomino, M., Ahn, E. E., Nagar, B., and Doan, N. (2019) Molecular mechanism of inhibition of acid ceramidase by carmofur. *J. Med. Chem.* **62**, 987–992

33. Lelieveld, L. T., Mirzaian, M., Kuo, C. L., Artola, M., Ferraz, M. J., Peter, R. E. A., Akiyama, H., Greimel, P., van den Berg, R., Overkleeft, H. S., Boot, R. G., Meijer, A. H., and Aerts, J. (2019) Role of beta-glucosidase 2 in aberrant glycosphingolipid metabolism: model of glucocerebrosidase deficiency in zebrafish. *J. Lipid Res.* **60**, 1851–1867

34. Artola, M., Kuo, C. L., Lelieveld, L. T., Rowland, R. J., van der Marel, G. A., Codee, J. D. C., Boot, R. G., Davies, G. J., Aerts, J., and Overkleeft, H. S. (2019) Functionalized cyclophellitols are selective glucocerebrosidase inhibitors and induce a Bona fide neuropathic Gaucher model in zebrafish. *J. Am. Chem. Soc.* **141**, 4214–4218

35. Rajput, V. B., Karthikeyan, M., and Ramasamy, S. (2019) Zebrafish acid ceramidase: expression in Pichia pastoris GS115and biochemical characterization. *Int. J. Biol. Macromol.* **122**, 587–593

36. Zhou, J., Tawk, M., Tiziano, F. D., Veillet, J., Bayes, M., Nolent, F., Garcia, V., Servidei, S., Bertini, E., Castro-Giner, F., Renda, Y., Carpentier, S., Andrieu-Abadie, N., Gut, I., Levade, T., *et al.* (2012) Spinal muscular atrophy associated with progressive myoclonic epilepsy is caused by mutations in ASAH1. *Am. J. Hum. Genet.* **91**, 5–14

37. Zhang, T., Trauger, S. A., Vidoudez, C., Doane, K. P., Pluimer, B. R., and Peterson, R. T. (2019) Parallel Reaction Monitoring reveals structure-specific ceramide alterations in the zebrafish. *Sci. Rep.* **9**, 19939

38. Marques, A. R., Mirzaian, M., Akiyama, H., Wisse, P., Ferraz, M. J., Gaspar, P., Ghauharali-van der Vlugt, K., Meijer, R., Giraldo, P., Alfonso, P., Irun, P., Dahl, M., Karlsson, S., Pavlova, E. V., Cox, T. M., *et al.* (2016) Glucosylated cholesterol in mammalian cells and tissues: formation and degradation by multiple cellular beta-glucosidases. *J. Lipid Res.* **57**, 451–463

39. Mirzaian, M., Wisse, P., Ferraz, M. J., Marques, A. R. A., Gaspar, P., Oussoren, S. V., Kytidou, K., Codee, J. D. C., van der Marel, G., Overkleeft, H. S., and Aerts, J. M. (2017) Simultaneous quantitation of sphingoid bases by UPLC-ESI-MS/MS with identical (13) C-encoded internal standards. *Clin. Chim. Acta.* **466**, 178–184

40. Guryev, V., Koudijs, M. J., Berezikov, E., Johnson, S. L., Plasterk, R. H., van Eeden, F. J., and Cuppen, E. (2006) Genetic variation in the zebrafish. *Genome Res.* **16**, 491–497

41. Mistry, P. K., Liu, J., Yang, M., Nottoli, T., McGrath, J., Jain, D., Zhang, K., Keutzer, J., Chuang, W. L., Mehal, W. Z., Zhao, H., Lin, A., Mane, S., Liu, X., Peng, Y. Z., *et al.* (2010) Glucocerebrosidase gene-deficient mouse recapitulates Gaucher disease displaying cellular and molecular dysregulation beyond the macrophage. *Proc. Natl. Acad. Sci. U. S. A.* **107**, 19473–19478

42. Filippi, A., Mahler, J., Schweitzer, J., and Driever, W. (2010) Expression of the paralogous tyrosine hydroxylase encoding genes th1 and th2 reveals the full complement of dopaminergic

ASBMB

and noradrenergic neurons in zebrafish larval and juvenile brain. *J. Comp. Neurol.* **518**, 423–438

43. Keatinge, M., Bui, H., Menke, A., Chen, Y. C., Sokol, A. M., Bai, Q., Ellett, F., Da Costa, M., Burke, D., Gegg, M., Trollope, L., Payne, T., McTighe, A., Mortiboys, H., de Jager, S., *et al.* (2015) Glucocerebrosidase 1 deficient danio rerio mirror key pathological aspects of human Gaucher disease and provide evidence of early microglial activation preceding alpha-synuclein-independent neuronal cell death. *Hum. Mol. Genet.* **24**, 6640–6652

44. Almagro Armenteros, J. J., Tsirigos, K. D., Sonderby, C. K., Petersen, T. N., Winther, O., Brunak, S., von Heijne, G., and Nielsen, H. (2019) SignalP 5.0 improves signal peptide predictions using deep neural networks. *Nat. Biotechnol.* **37**, 420–423

45. Madeira, F., Park, Y. M., Lee, J., Buso, N., Gur, T., Madhusoodanan, N., Basutkar, P., Tivey, A. R. N., Potter, S. C., Finn, R. D., and Lopez, R. (2019) The EMBL-EBI search and sequence analysis tools APIs in 2019. *Nucleic Acids Res.* **47**, W636–W641

46. Waterhouse, A., Bertoni, M., Bienert, S., Studer, G., Tauriello, G., Gumienny, R., Heer, F. T., de Beer, T. A. P., Rempfer, C., Bordoli, L., Lepore, R., and Schwede, T. (2018) SWISS-MODEL: homology modelling of protein structures and complexes. *Nucleic Acids Res.* **46**, W296–W303

47. McNicholas, S., Potterton, E., Wilson, K. S., and Noble, M. E. (2011) Presenting your structures: the CCP4mg molecular-graphics software. *Acta Crystallogr. D Biol. Crystallogr.* **67**, 386–394

48. Kinoshita, S., Biswas, G., Kono, T., Hikima, J., and Sakai, M. (2014) Presence of two tumor necrosis factor (tnf)-alpha homologs on different chromosomes of zebrafish (Danio rerio) and medaka (Oryzias latipes). *Mar. Genomics.* **13**, 1–9

49. Gaucher, P. C. E. (1882) De L'epithelioma Primitif de la Rate. Hypertrophie Idiopathique de la Rate Sans Leucemie, Paris, France

50. Stirnemann, J., Belmatoug, N., Camou, F., Serratrice, C., Froissart, R., Caillaud, C., Levade, T., Astudillo, L., Serratrice, J., Brassier, A., Rose, C., Billette de Villemeur, T., and Berger, M. G. (2017) A review of Gaucher disease pathophysiology, clinical presentation and treatments. *Int. J. Mol. Sci.* **18**, 441

51. Pandey, M. K., Burrow, T. A., Rani, R., Martin, L. J., Witte, D., Setchell, K. D., McKay, M. A., Magnusen, A. F., Zhang, W., Liou, B., Kohl, J., and Grabowski, G. A. (2017) Complement drives glucosylceramide accumulation and tissue inflammation in Gaucher disease. *Nature.* **543**, 108–112

52. Martins, R. R., Ellis, P. S., MacDonald, R. B., Richardson, R. J., and Henriques, C. M. (2019) Resident immunity in tissue repair and maintenance: the zebrafish model coming of age. *Front. Cell Dev. Biol.* **7**, 12

53. Enquist, I. B., Lo Bianco, C., Ooka, A., Nilsson, E., Mansson, J. E., Ehinger, M., Richter, J., Brady, R. O., Kirik, D., and Karlsson, S. (2007) Murine models of acute neuronopathic Gaucher disease. *Proc. Natl. Acad. Sci. U. S. A.* **104**, 17483–17488

54. Bosch, M. E., and Kielian, T. (2015) Neuroinflammatory paradigms in lysosomal storage diseases. *Front. Neurosci.* **9**, 417

55. Vardi, A., Ben-Dor, S., Cho, S. M., Kalinke, U., Spanier, J., and Futerman, A. H. (2020) Mice defective in interferon signaling help distinguish between primary and secondary pathological pathways in a mouse model of neuronal forms of Gaucher disease. *J. Neuroinflam.* **17**, 265

56. Blumenreich, S., Yaacobi, C., Vardi, A., Barav, O. B., Vitner, E. B., Park, H., Wang, B., Cheng, S. H., Sardi, S. P., and Futerman, A. H. (2021) Substrate reduction therapy using Genz-667161 reduces levels of pathogenic components in a mouse model of neuronopathic forms of Gaucher disease. *J. Neurochem.* **156**, 692–701

57. Milanese, C., Sager, J. J., Bai, Q., Farrell, T. C., Cannon, J. R., Greenamyre, J. T., and Burton, E. A. (2012) Hypokinesia and reduced dopamine levels in zebrafish lacking beta- and gammal-synucleins. *J. Biol. Chem.* **287**, 2971–2983

58. Uemura, N., Koike, M., Ansai, S., Kinoshita, M., Ishikawa-Fujiwara, T., Matsui, H., Naruse, K., Sakamoto, N., Uchiyama, Y., Todo, T., Takeda, S., Yamakado, H., and Takahashi, R. (2015) Viable neuronopathic Gaucher disease model in Medaka (Oryzias latipes) displays axonal accumulation of alpha-synuclein. *PLoS Genet.* **11**, e1005065

59. Srikanth, M. P., Jones, J. W., Kane, M., Awad, O., Park, T. S., Zambidis, E. T., and Feldman, R. A. (2021) Elevated glucosylsphingosine in Gaucher disease induced pluripotent stem cell neurons de-regulates lysosomal compartment through mammalian target of rapamycin complex 1. *Stem Cells Transl. Med.* **10**, 1081–1094

60. Vaz, R. L., Outeiro, T. F., and Ferreira, J. J. (2018) Zebrafish as an animal model for drug discovery in Parkinson's disease and other movement disorders: a systematic review. *Front. Neurol.* **9**, 347

61. Soria, F. N., Engeln, M., Martinez-Vicente, M., Glangetas, C., Lopez-Gonzalez, M. J., Dovero, S., Dehay, B., Normand, E., Vila, M., Favereaux, A., Georges, F., Lo Bianco, C., Bezard, E., and Fernagut, P. O. (2017) Glucocerebrosidase deficiency in dopaminergic neurons induces microglial activation without neurodegeneration. *Hum. Mol. Genet.* **26**, 2603–2615

62. Klein, A. D., Ferreira, N. S., Ben-Dor, S., Duan, J., Hardy, J., Cox, T. M., Merrill, A. H., Jr., and Futerman, A. H. (2016) Identification of modifier genes in a mouse model of Gaucher disease. *Cell Rep.* **16**, 2546–2553

63. Realini, N., Solorzano, C., Pagliuca, C., Pizzirani, D., Armirotti, A., Luciani, R., Costi, M. P., Bandiera, T., and Piomelli, D. (2013) Discovery of highly potent acid ceramidase inhibitors with in vitro tumor chemosensitizing activity. *Sci. Rep.* **3**, 1035

64. Ouairy, C. M., Ferraz, M. J., Boot, R. G., Baggelaar, M. P., van der Stelt, M., Appelman, M., van der Marel, G. A., Florea, B. I., Aerts, J. M., and Overkleeft, H. S. (2015) Development of an acid ceramidase activity-based probe. *Chem. Commun.* **51**, 6161–6163

65. Ordonez, Y. F., Abad, J. L., Aseeri, M., Casas, J., Garcia, V., Casasampere, M., Schuchman, E. H., Levade, T., Delgado, A., Triola, G., and Fabrias, G. (2019) Activity-based imaging of acid ceramidase in living cells. *J. Am. Chem. Soc.* **141**, 7736–7742

66. Rubboli, G., Veggiotti, P., Pini, A., Berardinelli, A., Cantalupo, G., Bertini, E., Tiziano, F. D., D'Amico, A., Piazza, E., Abiusi, E., Fiori, S., Pasini, E., Darra, F., Gobbi, G., and Michelucci, R. (2015) Spinal muscular atrophy associated with progressive myoclonic epilepsy: a rare condition caused by mutations in ASAH1. *Epilepsia.* **56**, 692–698

67. Ferraz, M. J., Marques, A. R., Gaspar, P., Mirzaian, M., van Roomen, C., Ottenhoff, R., Alfonso, P., Irun, P., Giraldo, P., Wisse, P., Sa Miranda, C., Overkleeft, H. S., and Aerts, J. M. (2016) Lyso-glyco-sphingolipid abnormalities in different murine models of lysosomal storage disorders. *Mol. Genet. Metab.* **117**, 186–193

68. Welford, R. W., Garzotti, M., Marques Lourenco, C., Mengel, E., Marquardt, T., Reunert, J., Amraoui, Y., Kolb, S. A., Morand, O., and Groenen, P. (2014) Plasma lysosphingomyelin demonstrates great potential as a diagnostic biomarker for Niemann-Pick disease type C in a retrospective study. *PLoS one.* **9**, e114669

69. Li, Y., Xu, Y., Benitez, B. A., Nagree, M. S., Dearborn, J. T., Jiang, X., Guzman, M. A., Woloszynek, J. C., Giaramita, A., Yip, B. K., Elsbernd, J., Babcock, M. C., Lo, M., Fowler, S. C., Wozniak, D. F., *et al.* (2019) Genetic ablation of acid ceramidase in Krabbe disease confirms the psychosine hypothesis and identifies a new therapeutic target. *Proc. Natl. Acad. Sci. U. S. A.* **116**, 20097–20103

70. Jeon, Y. J., Jung, N., Park, J. W., Park, H. Y., and Jung, S. C. (2015) Epithelial-mesenchymal transition in kidney tubular epithelial cells induced by globotriaosylsphingosine and globotriaosylceramide. *PLoS one.* **10**, e0136442

71. Rombach, S. M., van den Bogaard, B., de Groot, E., Groener, J. E., Poorthuis, B. J., Linthorst, G. E., van den Born, B. J., Hollak, C. E., and Aerts, J. M. (2012) Vascular aspects of Fabry disease in relation to clinical manifestations and elevations in plasma globotriaosylsphingosine. *Hypertension.* **60**, 998–1005

72. Sanchez-Nino, M. D., Sanz, A. B., Carrasco, S., Saleem, M. A., Mathieson, P. W., Valdivielso, J. M., Ruiz-Ortega, M., Egido, J., and Ortiz, A. (2011) Globotriaosylsphingosine actions on human glomerular podocytes: implications for Fabry nephropathy. *Nephrol. Dial. Transpl.* **26**, 1797–1802

73. Koch, B. E., Stougaard, J., and Spaink, H. P. (2014) Spatial and temporal expression patterns of chitinase genes in developing zebrafish embryos. *Gene Expr. Patterns.* **14**, 69–77

74. Nguyen-Ch, M., Laplace-Builhe, B., Travnickova, J., Luz-Crawford, P., Tejedor, G., Lutfalla, G., Kissa, K., Jorgensen, C., and Djouad, F. (2017) TNF signaling and macrophages govern fin regeneration in zebrafish larvae. *Cell Death Dis.* **8**, e2979

75. Harjula, S. E., Ojanen, M. J. T., Taavitsainen, S., Nykter, M., and Ramet, M. (2018) Interleukin 10 mutant zebrafish have an enhanced interferon gamma response and improved survival against a Mycobacterium marinum infection. *Sci. Rep.* **8**, 10360

76. Tang, R., Dodd, A., Lai, D., McNabb, W. C., and Love, D. R. (2007) Validation of zebrafish (Danio rerio) reference genes for quantitative real-time RT-PCR normalization. *Acta Biochim. Biophys. Sin. (Shanghai).* **39**, 384–390